MICROCOPY RESOLUTION TEST CHART
NATIONAL BUREAU OF STANDARDS-1963-A

AFWAL-TR-84-1075

COMPOUND SEMICONDUCTOR CHARACTERIZATION

DAVID C. LOOK, PH.D.
UNIVERSITY RESEARCH CENTER
WRIGHT STATE UNIVERSITY
DAYTON, OHIO 45435

8 JUNE 1984

Final Report for Period December 1980 - December 1983

Approved for public release; distribution unlimited.

AVIONICS LABORATORY
AIR FORCE WRIGHT AERONAUTICAL LABORATORIES
AIR FORCE SYSTEMS COMMAND
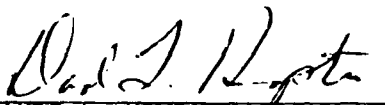WRIGHT-PATTERSON AIR FORCE BASE, OHIO 45433

DTIC
ELECTE
JUL 3 1 1984

B

84 07 2 015

NOTICE

When Government drawings, specifications, or other data are used for any purpose other than in connection with a definitely related Government procurement operation, the United States Government thereby incurs no responsibility nor any obligation whatsoever; and the fact that the Government may have formulated, furnished, or in any way supplied the said drawings, specifications, or other data, is not to be regarded by implication or otherwise as in any manner licensing the holder or any other person or corporation, or conveying any rights or permission to manufacture, use, or sell any patented invention that may in any way be related thereto.
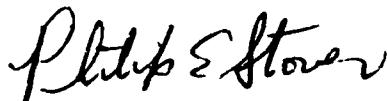
This report has been reviewed by the Office of Public Affairs (ASD/PA) and is releasable to the National Technical Information Service (NTIS). At NTIS, it will be available to the general public, including foreign nations.

This technical report has been reviewed and is approved for publication.

DAVID L. KINGSTON
Program Manager
Electronic Research Branch

FOR THE COMMANDER

PHILIP E. STOVER, Chief
Electronic Research Branch
Avionics Laboratory

REPORT DOCUMENTATION PAGE		READ INSTRUCTIONS BEFORE COMPLETING FORM
1. REPORT NUMBER AFWAL-TR-84-1075	2. GOVT ACCESSION NO. AD.A143601	3. RECIPIENT'S CATALOG NUMBER
4. TITLE (and Subtitle) COMPOUND SEMICONDUCTOR CHARACTERIZATION		5. TYPE OF REPORT & PERIOD COVERED FINAL REPORT DECEMBER 1980 – DECEMBER 1983
		6. PERFORMING ORG. REPORT NUMBER
7. AUTHOR(s) DAVID C. LOOK, PHIL WON YU, SANG BOO NAM, DENNIS C. WALTERS, SIDDHESWAR CHAUDHURI		8. CONTRACT OR GRANT NUMBER(s) F33615-81-C-1406
9. PERFORMING ORGANIZATION NAME AND ADDRESS UNIVERSITY RESEARCH CENTER WRIGHT STATE UNIVERSITY DAYTON, OHIO 45435		10. PROGRAM ELEMENT, PROJECT, TASK AREA & WORK UNIT NUMBERS P. E. 61102F 2306R111
11. CONTROLLING OFFICE NAME AND ADDRESS AVIONICS LABORATORY (AFWAL/AADR) AIR FORCE WRIGHT AERONAUTICAL LABORATORIES WRIGHT-PATTERSON AFB, OH 45433		12. REPORT DATE 8 JUNE 1984
		13. NUMBER OF PAGES 94
14. MONITORING AGENCY NAME & ADDRESS(If different from Controlling Office)		15. SECURITY CLASS. (of this report) UNCLASSIFIED
		15a. DECLASSIFICATION/DOWNGRADING SCHEDULE

16. DISTRIBUTION STATEMENT (of this Report)

APPROVED FOR PUBLIC RELEASE; DISTRIBUTION UNLIMITED.

17. DISTRIBUTION STATEMENT (of the abstract entered in Block 20, if different from Report)

18. SUPPLEMENTARY NOTES

19. KEY WORDS (Continue on reverse side if necessary and identify by block number)

GaAs	III-V Compounds	Type Conversion	Local Vibrational Mode
Antisite	Semi-insulating	Quantum Well	Photoluminescence
Soliton	Ion Implantation	Velocity-Field	Mass Spectroscopy
Statistics	Native Defects	Compensation	Superconductivity
Profiling	Hall Effect	Heterostructure	Transport Theory
			Field Effect Transistor

20. ABSTRACT (Continue on reverse side if necessary and identify by block number)

Impurities and defects in semiconducting and semi-insulating GaAs and other III-V compounds have been investigated by electrical, optical, and mass spectroscopic techniques. Field-effect transistors have been fabricated and tested.

FOREWORD

The work described in this report covers the period 16 December 1980 –
31 December 1983, and involved approximately 22 man-years of effort. The
personnel contributing for all or part of the time include: Dr. David C.
Look, Dr. Phil Won Yu, Dr. Sang Boo Nam, Dr. Siddheswar Chaudhuri,
Dr. William M. Theis, Dr. Krishan K. Bajaj, Mr. Dennis C. Walters,
Mr. Timothy A. Cooper, Mr. John E. Hoelscher, and Mr. Gregory W. Smith.
Administrative matters were ably handled by Dr. Donald C. Thomas, Mr. Jess
E. Anderson, and Dr. Mark Sirkin, all of the Wright State University School
of Graduate Studies. Secretarial duties were efficiently performed by
Mrs. Patricia Winship. We also wish to thank our many colleagues at the
Air Force Avionics Laboratory who provided an excellent working environment.
Our special gratitude goes to Mr. David L. Kingston, the contract monitor,
and Dr. Phillip Stover, the branch chief.

This work was performed by the Wright State University School of
Graduate Studies, Oelman Hall, Col. Glenn Highway, Dayton, Ohio, 45435,
under Contract F33615-81-C-1406. The project, task, and work unit number
was 2306R101, and the project engineer was David L. Kingston, AFWAL/AADR,
Wright-Patterson AFB, Ohio, 45433. The report was submitted on 31 January
1984.

DTIC
ELECTE
JUL 3 1 1984

B

Accession For

NTIS GRA&I
DTIC TAB
Unannounced
Justification

By
Distribution/
Availability Codes

Dist	Avail and/or Special
A-1	

iii

TABLE OF CONTENTS

TABLE OF CONTENTS

LIST OF FIGURES

LIST OF FIGURES

LIST OF TABLES

1.0 ELECTRICAL PROPERTIES OF CONDUCTING GALLIUM ARSENIDE

1.1 Introduction

The two basic parameters determined in electrical-measurement studies are the carrier concentration (n or p) and the carrier mobility (μ_n or μ_p). (Hereafter, we will refer only to n and μ_n unless we are specifically dealing with p-type samples.) The most common experiment used to ascertain n and μ_n is the Hall-effect, along with conductivity. To use the Hall-effect in the most accurate manner, it is necessary to know the Hall r-factor, defined by n = r/eR, where R is the Hall coefficient.[1] Then, once n is known accurately, it must be properly related to the real quantities of interest, namely, the donor and acceptor concentrations (N_D and N_A, respectively), and their energies with respect to the relevant band (E_D and E_A, respectively). However, at the beginning of this contract it was clear that neither of these subjects was being handled well in common practice. For example, nearly all researchers simply dealt with the first problem by assuming r = 1, and with the second, by assuming K = 1, 4, or ½ in the distribution function for donors or acceptors:

$$f(\omega) = 1/[1 + K \exp (\omega - \omega_F)/ k T] \tag{1-1}$$

where ω is the energy of an electron and ω_F is the Fermi energy. However, even the form of Eq. 1-1 is wrong if a bound center has more than one charge state within the band gap, or important excited states. Thus, we realized that some theoretical work was needed before any serious conclusions could be drawn from our electrical measurements. Also, hole transport theory is even in much worse shape than electron transport theory, and we were able to make some improvements here, although nothing fundamental.

We applied these concepts to a number of problems in conducting GaAs, including: (1) a detailed analysis of low-compensation vapor-phase-epitaxial (VPE) GaAs; (2) the identification of two prominent centers at

1

E_c -0.15 eV, and E_c -0.43 eV, as pure defects; and (3) the development of mobility profiling techniques for conductive FET layers. These problems will be discussed in detail below.

1.2 Statistics of Multi-Charge Centers in Semiconductors

Most researchers seriously involved with electrical measurements, and in particular with temperature-dependent Hall-effect measurements, have experienced trouble with choosing or determining a degeneracy factor, i.e., the "K" of Eq. 1-1. Thus, we dealt with this problem and derived the following general formulas:[2]

$$n_{k\ell m} = \frac{N_k}{1 + \sum_{\ell',m' \neq \ell,m} \frac{g_{k\ell'm'}}{g_{k\ell m}} e^{\eta_{k\ell m} - \eta_{k\ell'm'} - (\ell-\ell')\eta_F}} \qquad (1-2)$$

$$n = p + \sum_{k,\ell,m} (\ell_k - \ell) n_{k\ell m} \qquad (1-3)$$

where N_k is the concentration of type-k donors or acceptors, ℓ_k is the number of ionizable electrons (with less than band-gap energy) on a center of type-k, "m" denotes excited states, $g_{k\ell m}$ is the degeneracy of the $k\ell m\underline{\text{th}}$ state, $\eta_{k\ell m} = \mathcal{E}_{k\ell m}/kT$, and $\ell = 0, 1, -- \ell_k$. The restriction on the summation means that $\ell \neq \ell'$ and $m \neq m'$, at the same time. Equations 1-2 and 1-3 are completely general for any number of donors and acceptors with any numbers of ionizable electrons and excited states. Note that Eq. 1-3 is simply the charge-balance equation. Many examples of the application of these equations are given in References 1 and 2.

2

1.3 Electron Transport Theory

To properly use Equations 1-2 and 1-3, we must know n (or p, for

p-type samples), as a function of temperature. From a Hall-effect measure-

ment we get $n = r/eR$, where R is the measured quantity, but r is unknown.

Most researchers simply set $r = 1$, which is justified for rough measure-

ments, since $1 \lesssim r \lesssim 1.3$ in the usual GaAs samples. However, to do better,

we must either measure R at very high magnetic fields (such that $\mu(cm^2/V\text{-sec})$

B (gauss) $\gg 10^8$), or else calculate r from mobility measurements, fitted

to scattering theory. For relatively pure GaAs, in the room-temperature

range, polar optical-mode scattering is dominant, and it is necessary to

solve the Boltzmann transport equation by numerical means. We have adopted

a program written by Nag[3], who uses Rode's[4] iterative solution of the

Boltzmann equation. Modifications to Nag's program include the considera-

tion of neutral impurities in both scattering and screening. The use of

this program to fit data is presented in a later section. Recently, we

have also modified the ionized-impurity scattering, by incorporating the

work of Meyer and Bartoli[5]. Various unknown parameters, such as the

acoustic-deformation-potential constant, have been determined by fitting

to two pure VPE layers, grown at AFWAL/AADR by Peter C. Colter. Thus, we

feel that our mobility fitting program is probably one of the most complete

in existence, at the present time. Much of the computer programming for

this project has been carried out by John R. Sizelove, AFWAL/ADO.

1.4 Hole Transport Theory

The following abstract is reprinted from Ref. 6.

We have used a two-band model (heavy and light holes) to calculate
the transport properties of p-type GaAs. The scattering mechanisms
included are acoustic-mode deformation potential, acoustic-mode piezo-
electric potential, polar- and nonpolar-mode deformation potential, ionized
impurity, and space charge. Interband scattering is included explicity for
the optical phonons and phenomenologically for the acoustic phonons. The
intraband polar optical-mode scattering, for which a relaxation time cannot
be defined, was calculated by using the numerical method of Fletcher and
Butcher. The acoustic deformation-potential parameter and the coupling
coefficient for interband scattering were calculated by fitting the theory
to Hall-mobility data for both pure and doped samples. We have determined
ionized-impurity and space-charge contributions for two of our samples, one
doped with Cr and exhibiting an 0.33-eV activation energy (Cr^{4+}/Cr^{3+}), and
the other heat-treated and exhibiting an 0.14-eV activation energy. The
transport fit was carried out self-consistently with a statistical fit of
the p vs T data, to determine the relevant donor and acceptor concentrations.
Individual plots of the mobility contributions from the various scattering
mechanisms are also presented. Finally, useful plots of the Hall mobility
and Hall r factor, as functions of carrier density and compensation ratio,
are provided to aid others in the analysis of their samples. An important
conclusion of this study is that the light-hole band strongly influences the
transport properties, even though its density of states is small compared to
that of the heavy-hole band.

1.5 Electrical Properties of Low-Compensation GaAs

It was found by P. C. Colter, of this laboratory, that very low receptor concentrations could be obtained in VPE GaAs by baking the Ga source prior to growth to reduce Zn contamination, and by taking other precautions to reduce deep levels. Because of the uniqueness of these samples, a very careful electrical-measurement study was in order. First we measured R vs. T in an automated Hall-effect system, developed earlier[7]. Then we determined n from the relationship $n = r/eR$, where $r(T)$ was calculated from our mobility-fitting program. Finally, we fitted n vs. T to the following charge-balance equation, developed from Equations 1-1 and 1-2:

$$n + N_A = N_D / (1 + n/\phi) \qquad (1-4)$$

where

$$\phi = \frac{2(2\pi m_n^* kT)^{3/2}}{h^3} \frac{g_o}{g_1} e^{\alpha/k} T^{3/2} e^{-E_{DO}/T} \qquad (1-5)$$

Here the donor energy is defined by $E_D = E_{DO} - \alpha T$, and g_o and g_1 are the degeneracies of the unoccupied and occupied donor states, respectively. From the n vs. T fit we get the parameters N_D, N_A, E_{DO}, and (g_o/g_1) exp (α/k). We also get N_A from the mobility fit. The experimental and theoretical curves of μ_n and n are presented in Figures 1-1 and 1-2, respectively, and the fitted parameters, in Table 1-1. Both the acceptor concentration, and the compensation ratio (N_A/N_D), are the lowest ever reported for GaAs.

For further details of this work, see Ref. 8.
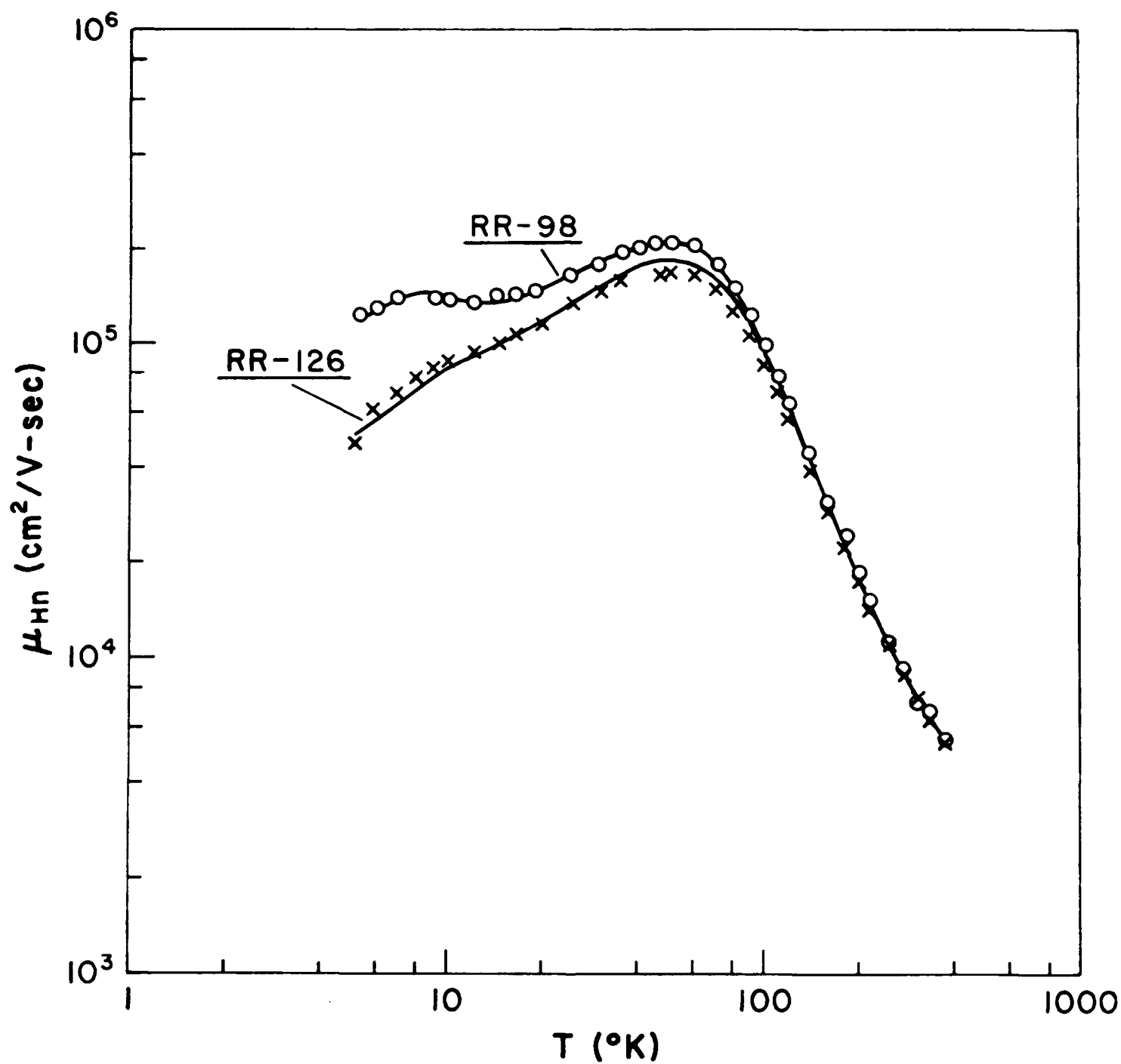
Fig. 1-1 Hall mobility vs. temperature data and theoretical fits
for two VPE GaAs samples.
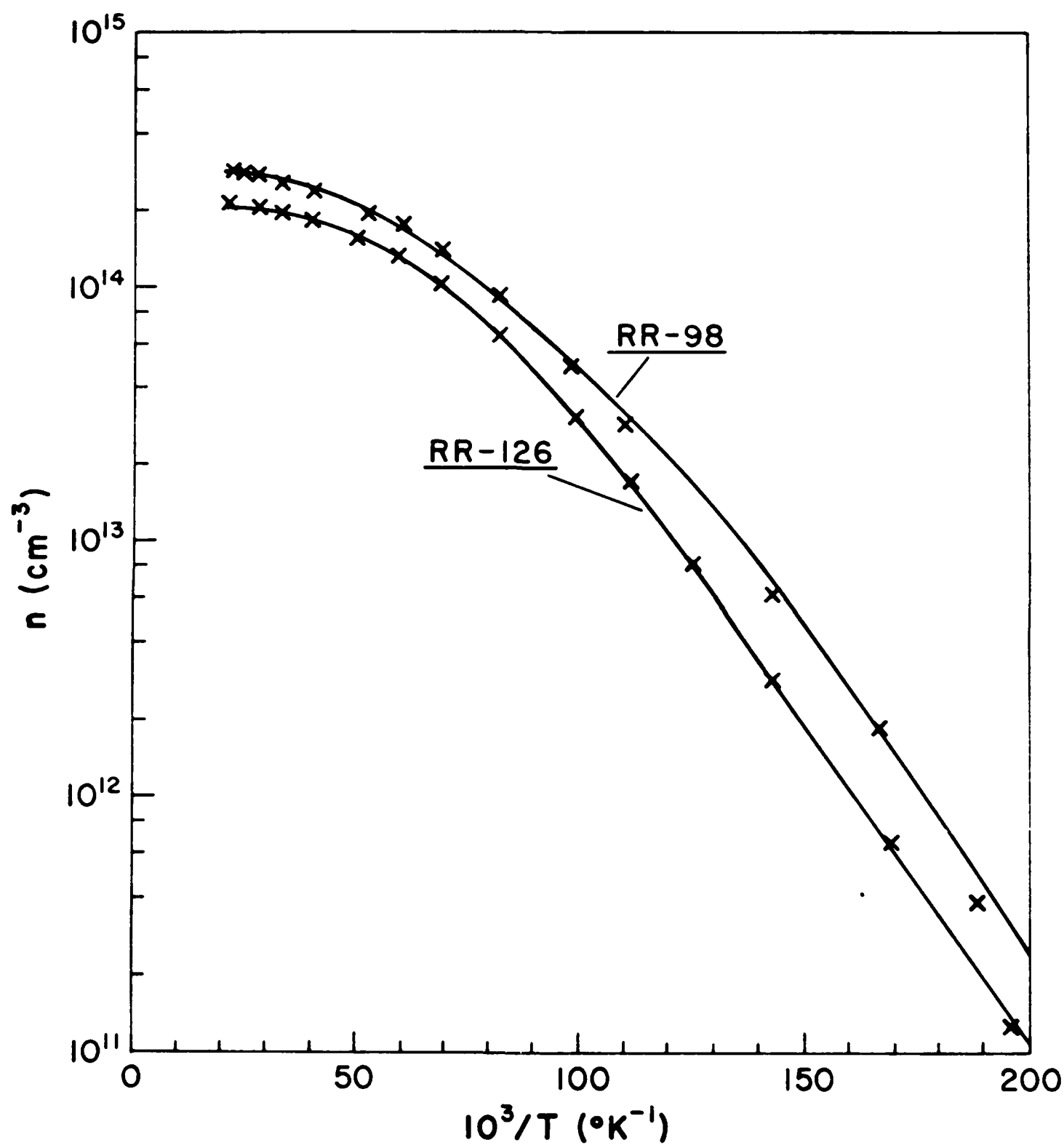
Fig. 1-2 Electron concentration (corrected for Hall scattering factor) vs. temperature data and theoretical fits for two VPE GaAs samples.

TABLE 1-1. Fitted parameters from n vs T and μ_{Hn} vs T data.

Sample	μ_{Hn} vs T N_A (cm^{-3})	n vs T N_A (cm^{-3})	N_D (cm^{-3})	E_{DO} (meV)	Best value N_A (cm^{-3})	N_A/N_D
RR-98	1.5×10^{13}	2.5×10^{13}	3.1×10^{14}	4.7	$(2 \pm 1) \times 10^{13}$	0.06 ± 0.03
RR-126	7.8×10^{13}	1.1×10^{14}	3.2×10^{14}	4.3	$(9 \pm 3) \times 10^{13}$	0.28 ± 0.09

1.6 Defect Centers in GaAs

As crystal growers have been able to reduce impurity contamination in GaAs, the intrinsic defects have become more important. Although many such defect energy levels have been found in electron- or ion-irradiated samples, none of these has ever been proven dominant in as-grown material. (There is, however, now a strong belief that the dominant deep donor (EL2) in undoped, semi-insulating LEC material, is indeed the anion antisite defect As_{Ga}.) In general, n-type, bulk, as-grown GaAs is dominated by one of three levels: (1) the shallow, hydrogenic levels, such as Si_{Ga} or Se_{As}; (2) an 0.15 eV level; and (3) an 0.43 eV level. We have shown by a combination of electrical and analytical techniques that the latter two are pure defects, not associated with any impurities. The technological importance of this result is that further reductions of donor and acceptor concentrations in bulk GaAs will have to be concerned with defects as much as impurities.

Further details may be found in References 9 and 10.

1.7 Mobility Profiling in FET Layers

Although carrier-concentration profiles in semiconductor layers have been routinely extracted for years, by capacitance-voltage (C-V) measurements on Schottky barriers, it is much more difficult to measure mobility profiles. Two methods which have been developed include: (1) the Hall-effect method, in which a reverse-biased Schottky barrier is used to successively deplete the conductive layer[11]; and (2) the FET geometric magnetoresistance (GMR) method, in which the magnetic-field dependence of the source-drain (SD) current is measured as the reverse-bias gate voltage is increased, in steps[12, 13]. We have developed a fully automated apparatus to carry out both of these techniques. The

9

GMR technique is simpler in that only one parameter must be measured, namely the S-D current, as long as gate current is negligible. However, to obtain data close to the surface, it is necessary to forward-bias the FET, and then gate current can become important. We have developed an FET circuit model in which gate current is properly taken into account. If it is impossible to measure the gate current, then there are ways to minimize its effect, e.g., by averaging I_{SD} readings for V_{SD} and $-V_{SD}$. In Fig. 1-3 we show the carrier concentration and mobility profiles in a FAT FET, for which the gate current is actually larger than the S-D current, in the most forward-bias mode. It is seen that the mobility correction is very large in this region. With these corrections, we are now able to get accurate mobility data much closer to the surface than before.
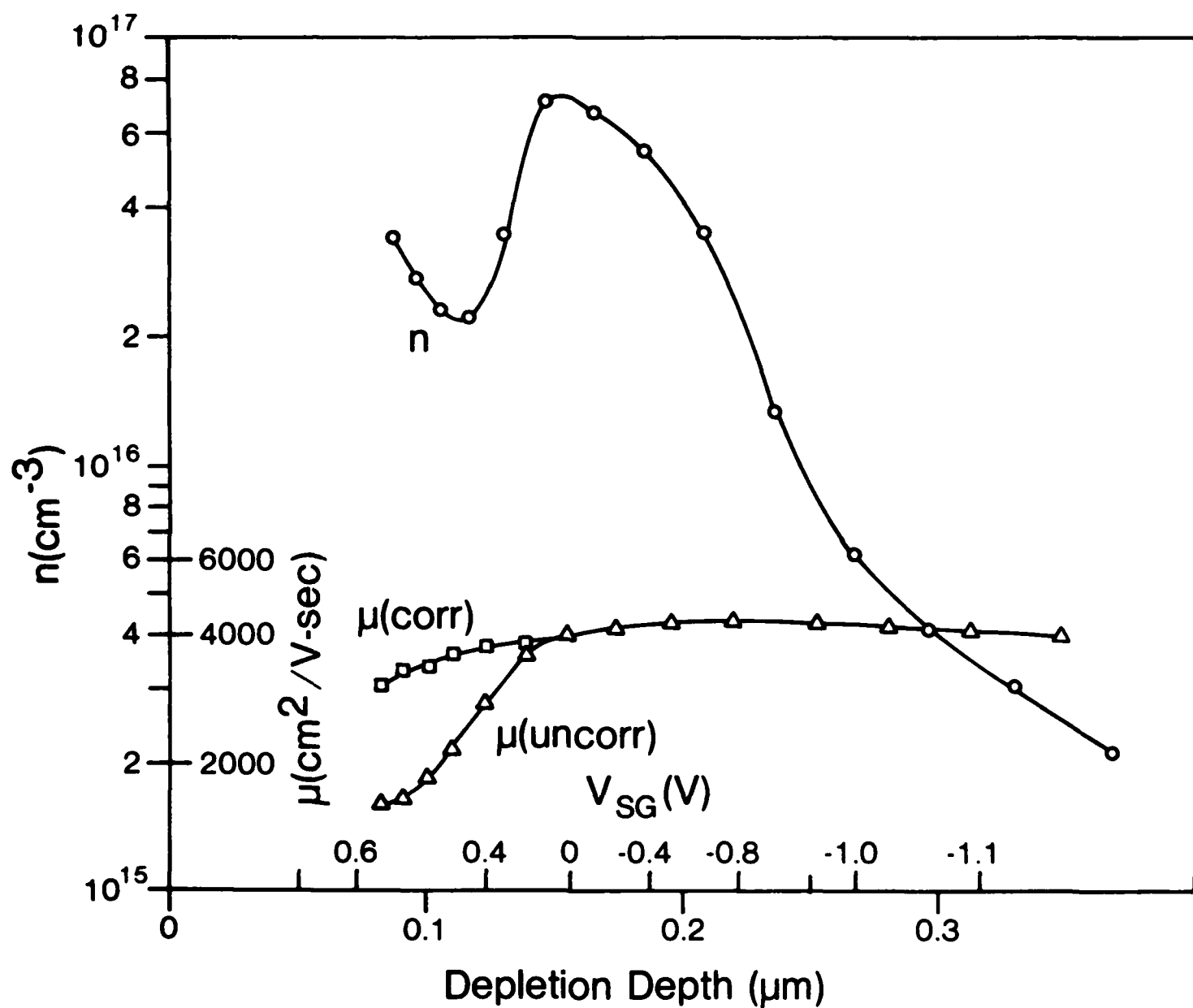
Fig. 1-3 The electron concentration and mobility for a semi-insulating GaAs substrate implanted with $4 \times 10^{12}/cm^2$, 100 keV Si ions, and annealed at 850°C for 15 min.

2.0 ELECTRICAL PROPERTIES OF SEMI-INSULATING GALLIUM ARSENIDE

2.1 Introduction

A big advantage in the development of GaAs IC technology is the existence of semi-insulating (SI) forms of GaAs, namely those containing Cr, or the defect, EL2. Thus, it is possible to grow good single-crystal epitaxial layers, or form a conductive layer by implantation, and not have to worry about the "platform," namely the S I GaAs. Unfortunately, this optomistic picture has not been fully realized, as yet, for various reasons. The importance of the S I GaAs problem is demonstrated by the calling of international conferences on the subject in 1980, 1982, and in 1984 (coming up). Thus, we have devoted a large part of our effort to this subject and have made both theoretical and experimental contributions. The highlights include: (1) discovery of a donor transition (Cr^{3+}/Cr^{4+}) in Cr-doped GaAs; (2) showing that an 0.1 eV "conversion" center is not always Mn, as commonly believed; and (3) correlating SI substrate properties with the device (FET) properties.

2.2 Magneto-Hall and Magnetoresistance Coefficients in Semiconductors with Mixed Conductivity

The electrical properties of Cr-doped GaAs are complicated by the existence of both hole and electron conductivity, since the Fermi level is near the middle of the band gap. Thus, four unknowns exist: n, p, μ_n, and μ_p. The problem can be solved exactly by measuring the second-order magnetic field dependences of the conductivity and Hall coefficient, if all of the magnetic-field dependence of these parameters is due to mixed-conductivity effects.[14] However, if single-carrier magnetic-field dependences are also large, then the problem is much more complicated. We have developed detailed expressions, to order $\mu^2 B^2$, for the

12

magnetoresistance and magneto-Hall coefficients, allowing both single-carrier and mixed-carrier effects. The expressions are too lengthy to be presented here, but further details may be found in Ref. 15.

2.3 Discovery of the Cr^{4+}/Cr^{3+} Donor Transition in GaAs

Temperature-dependent Hall-effect measurements on two Cr-doped GaAs samples show a dominant center at $E_1 = 0.324-1.4 \times 10^{-4}T$ eV, with respect to the valence-band edge. By comparison with secondary-ion mass spectroscopy measurements of the Cr concentration, and recent EPR measurements of the Cr^{2+}, Cr^{3+}, and Cr^{4+} concentration in several samples, it is shown unambiguously that this energy describes the $Cr^{4+} \rightarrow Cr^{3+}$ transition. This is the first conclusive evidence for a charge-state transition involving Cr^{4+} in GaAs. The technological importance of this result is that to produce p-type material say by implantation of N_A acceptors, in Cr-doped material, we must have $N_A > N_D + N_{Cr}$, not just $N_A > N_D$, which would be the case if Cr did not have a donor transition.

Further information may be found in Ref. 16.

2.4 The 0.1 eV Conversion Center in GaAs

The existence of a semi-insulating (SI) form of GaAs has been essential for the development of much of the present-day GaAs device technology.[17] A well-known problem with SI GaAs, however, is the "conversion" phenomenon, in which a thin, conducting surface layer is formed upon heating to the temperatures required for expitaxial growth, or ion-implantation annealing. One of the most common types of conversion involves a p-type layer which exhibits a thermal (Hall-effect) activation energy of 0.1 eV, and a photoluminescence line at 1.41 eV. Such a layer is formed, e.g., by annealing SI GaAs in H_2 gas at 700-800°C. The relevant acceptor has been

13

attributed to Mn_{Ga},[18-23] $Si_{As} - V_{As}$,[24-27] $C_{As} - V_{As}$,[26-28] and V_{As}.[29] In an attempt to study this problem further, Yu and Park[20] have compared the shapes and temperature dependences of the respective 1.41-eV emission lines from Mn-implanted samples, and unimplanted, annealed SI samples. The results were nearly identical. Thus, we feel that Mn_{Ga} represents the most likely cause of the 1.41-eV emission in the majority of annealed samples investigated to date, although the other possibilities, mentioned above, cannot be ruled out in all cases.

We report here a rather extensive investigation of two semi-insulating liquid-encapsulated Czochralski crystals, one undoped (sample F) and the other Cr doped (sample G). Both samples were annealed at $750^{\circ}C$, face up, for 15 min. in an H_2 ambient, to simulate vapor-phase epitaxial (VPE) growth conditions. The surfaces appeared unchanged after the anneals. This treatment produced, in each case, a p-type layer with a sheet resistivity of about $10^5 \, \Omega / \Box$, due to a dominant acceptor level about 0.1 eV from the valence band. Also, a 1.41-eV emission line was observed. However, we will show that the acceptor is definitely not related to Mn, even though the 1.41-eV emission probably is. Thus, the elimination of Mn from the substrate and growth ambient will not eliminate conversion, at least not in all cases. Indeed, it appears that a defectlike state may be the most important constituent of the 0.1-eV center.

14

2.5 The Effects of SI GaAs Substrates on FET Devices

The following abstract is reprinted from Ref. 30.

A detailed investigation of 21 SI GaAs substrates, Cr-doped, oxygen-doped, and undoped, Bridgman and Czochralski, from 8 different manufacturers, has been carried out by temperature-dependent Hall effect (TDH), differential Hall effect (DH), photoluminescence, spark-source mass spectroscopic and secondary-ion mass spectroscopic measurements. Also, Se-ion-implanted MESFET's, with 4 μm gates, were fabricated on several of the substrates and tested. Electrical conversion tests were carried out to simulate typical VPE growth conditions (750°C, 15 min., hydrogen atmosphere, no cap), and ion-implantation annealing conditions (900°C, 15 min., hydrogen atmosphere, Si_3N_4 cap). The following conclusions have emerged from this study: (a) It is very difficult to get reliable n-type activation at less than the mid-10^{17} cm^{-3} level, at least with 120 Ke V Se ions. (b) Low mobilities ($\leqslant 10^3 cm^2$ $V^{-1}s^{-1}$), often seen in SI GaAs substrate materials, are due to inhomogeneity (if $\rho \leqslant 4 \times 10^8$ Ω cm). The effective channel mobilities in implanted MESFET's, near pinch-off, are heavily influenced by these low substrate mobilities. (c) The commonly observed 0.5 eV acceptor conversion level is due to Fe, but the 0.1 eV acceptor level is not always due to Mn, as evidently believed by many workers.

3.0   PHOTOLUMINESCENCE IN SEMI-INSULATING GALLIUM ARSENIDE

3.1 Introduction

A major impediment to the development of GaAs integrated circuits

and microwave devices has been the lack of a reliable supply of semi-insu-

lating substrates. The main question surrounding semi-insulating GaAs has

concerned the compensation mechanism by which the undoped material is

semi-insulating. The understanding of the compensation mechanism has two

important practical consequences. First, knowledge of cause-effect

relationships between crystal growth and material properties would greatly

improve the yield of semi-insulating crystals. Second, this understanding

would greatly improve the device performance.

It is well known that the main deep donor located at ~ 0.75 eV

from the conduction band is present in GaAs materials and that this donor

is primarily responsible for semi-insulating properties through certain

compensation mechanisms. In our study, deep center luminescence has been

studied through the change of temperature, the persistent photoluminescence

quenching effect, and the stoichiometry of crystals, in order to identify

the radiative mechanisms involved in deep centers in undoped and Cr-doped

semi-insulating materials.

3.2 Characteristics of Undoped Semi-insulating GaAs (Ref. 31)

A photoluminescence emission study has been made on undoped LEC

GaAs crystals grown from gallium- and arsenic-rich melts. A 77-meV deep

acceptor responsible for the 1.44-eV emission is present both in p-type

conducting and n-type semi-insulating crystals. The 0.68- and 0.77-eV

emissions present in the semi-insulating materials are explained in terms

of the radiative transitions between the band edge and deep centers.

Figure 3-1 shows the typical deep-center photoluminescence emission from

n-type semi-insulating GaAs.

16
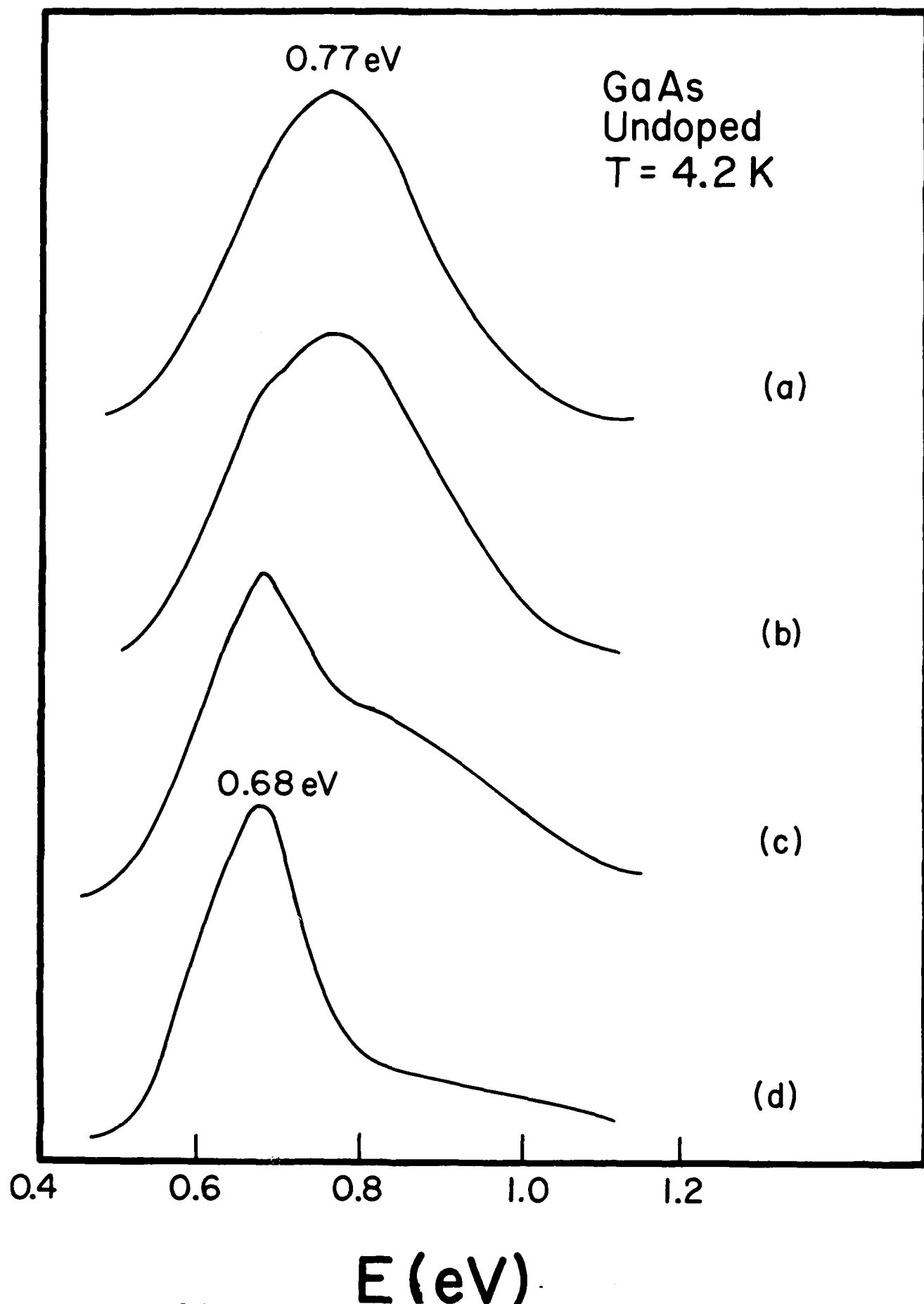
Fig. 3-1 Deep-center emission characteristics obtained from
n-type semi-insulating crystals.

3.3 Temperature Dependence of 0.68-eV Band in GaAs (Ref. 32)

The 0.68 eV photoluminescence band present in undoped semi-insulating GaAs crystals has been studied[32] with the change of temperature. It is shown that the 0.68 eV band is due to the radiative transition involving a main deep donor and the valence band. The origin of the donor is intrinsic and may involve an As antisite defect. It is found that the donor level does not change in energy with respect to the valence band at T = 4-300 K. The donor level is found to be at 0.73 eV from the conduction band at T = 4K. The temperature dependence of the 0.68-eV band at different temperatures is shown in Figure 3-2. The temperature dependence of the half-width for two samples is also illustrated in Figure 3-3.

3.4 Quenching Behavior of 0.68-eV Band in GaAs (Ref. 33)

The persistent photoluminescence quenching effect is shown to occur on the broad 0.68-eV emission commonly present in undoped semi-insulating GaAs bulk materials. The dependence of this persistent emission on below band-gap energy excitation has been measured. The data indicate involvement of the main deep donor EL2 in the radiative mechanism of the 0.68-eV emission. The persistent photoluminescence quenching effect can be explained by the presence of both normal and metastable states of EL2. Figure 3-4 shows the 0.68-eV band photoluminescence quenching rate vs. below-bandgap-excitation energy.

3.5 0.63-eV Band Related to Oxygen in GaAs (Ref. 34 and 35)

Temperature-dependent photoluminescence and photoluminescence excitation spectroscopy have been used to measure the 0.63-eV luminescence band present in O-doped semi-insulating GaAs. It is shown that the 0.63-eV band is related to the presence of O. The center responsible for the band forms a deep level similar to the main deep donor EL2. However, spark

18
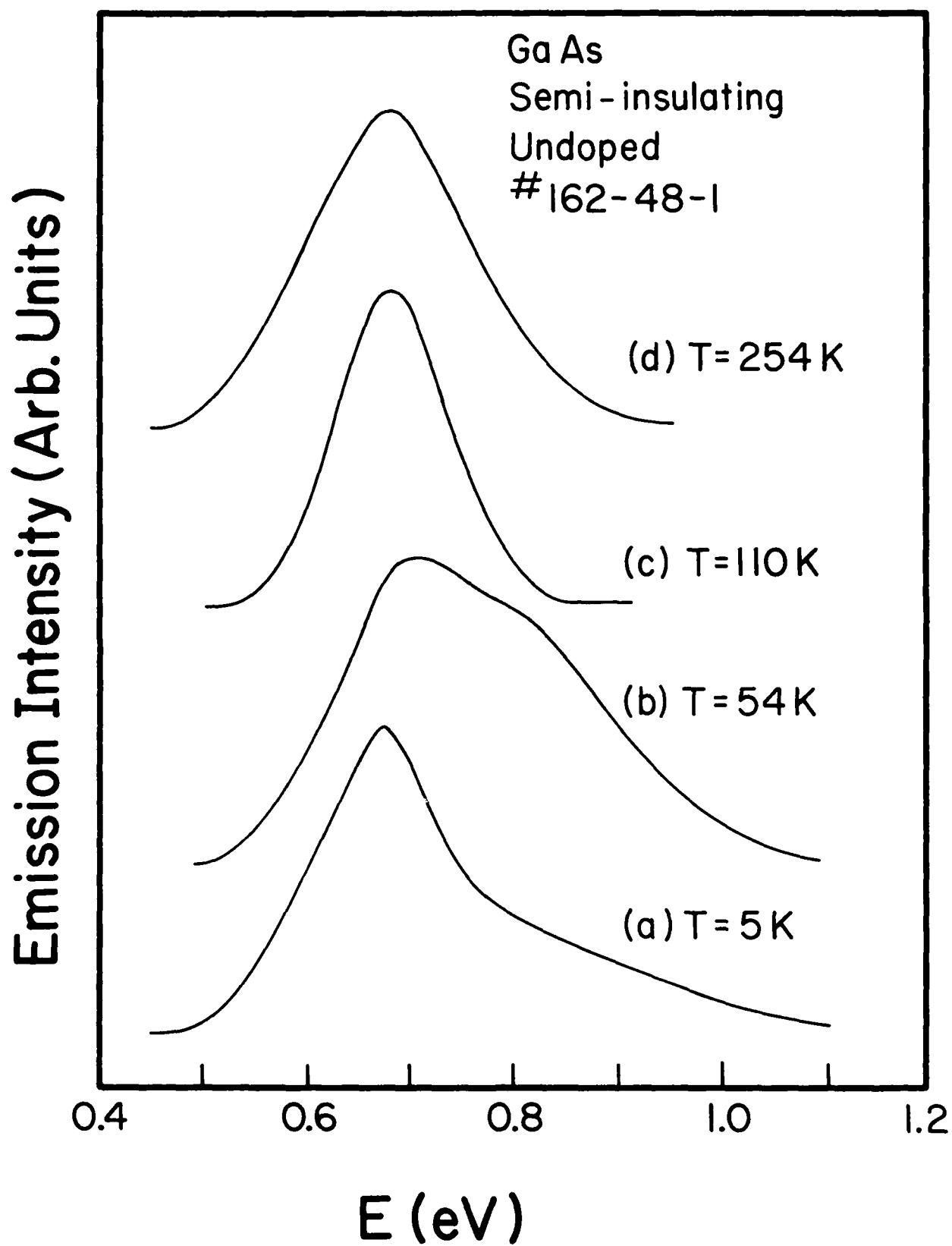
Fig. 3-2   Temperature dependence of the 0.68-eV band at T = 5, 54, 110 and 254 K.
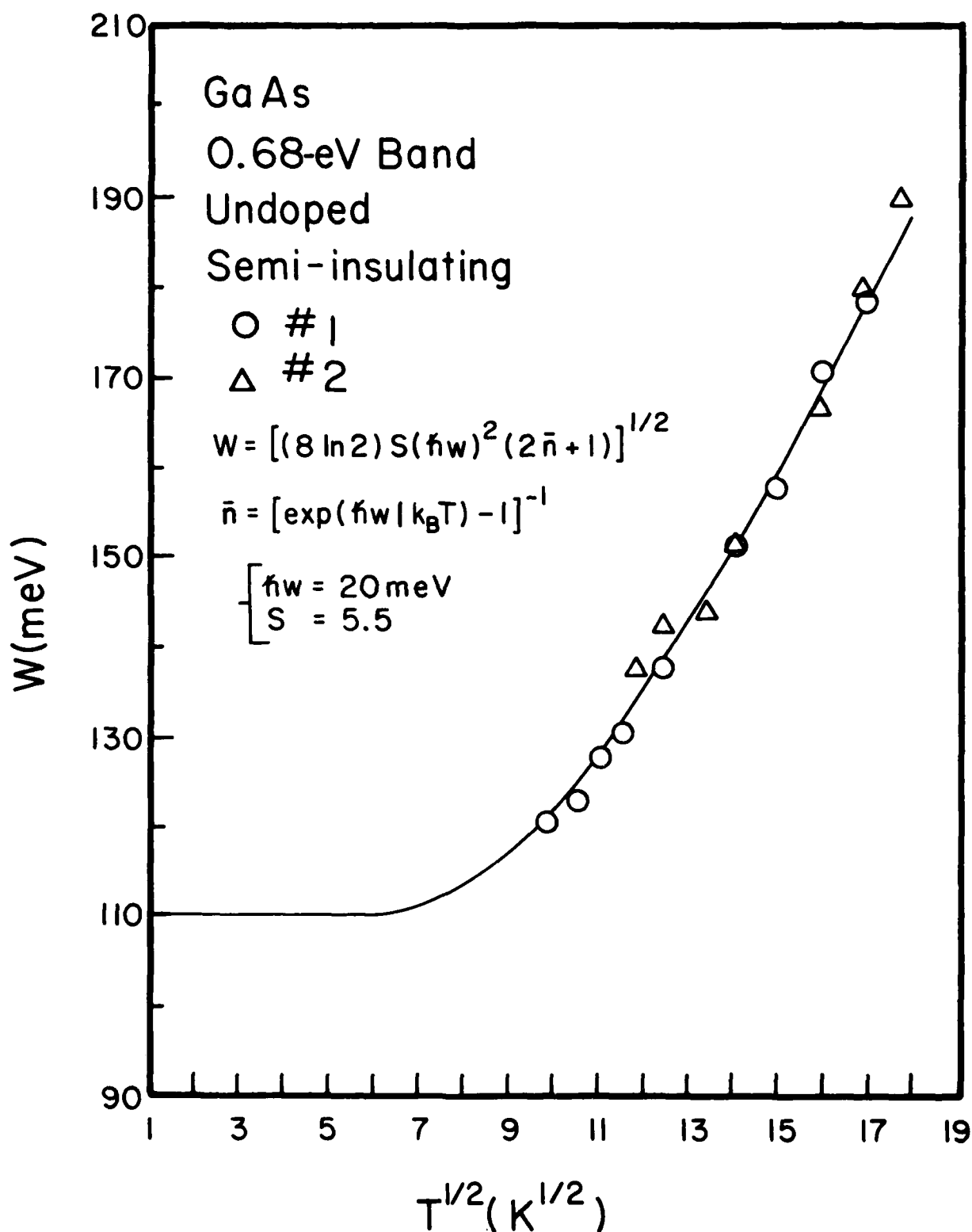
Fig. 3-3 Temperature dependence of the half-width of the 0.68-eV band for two samples.
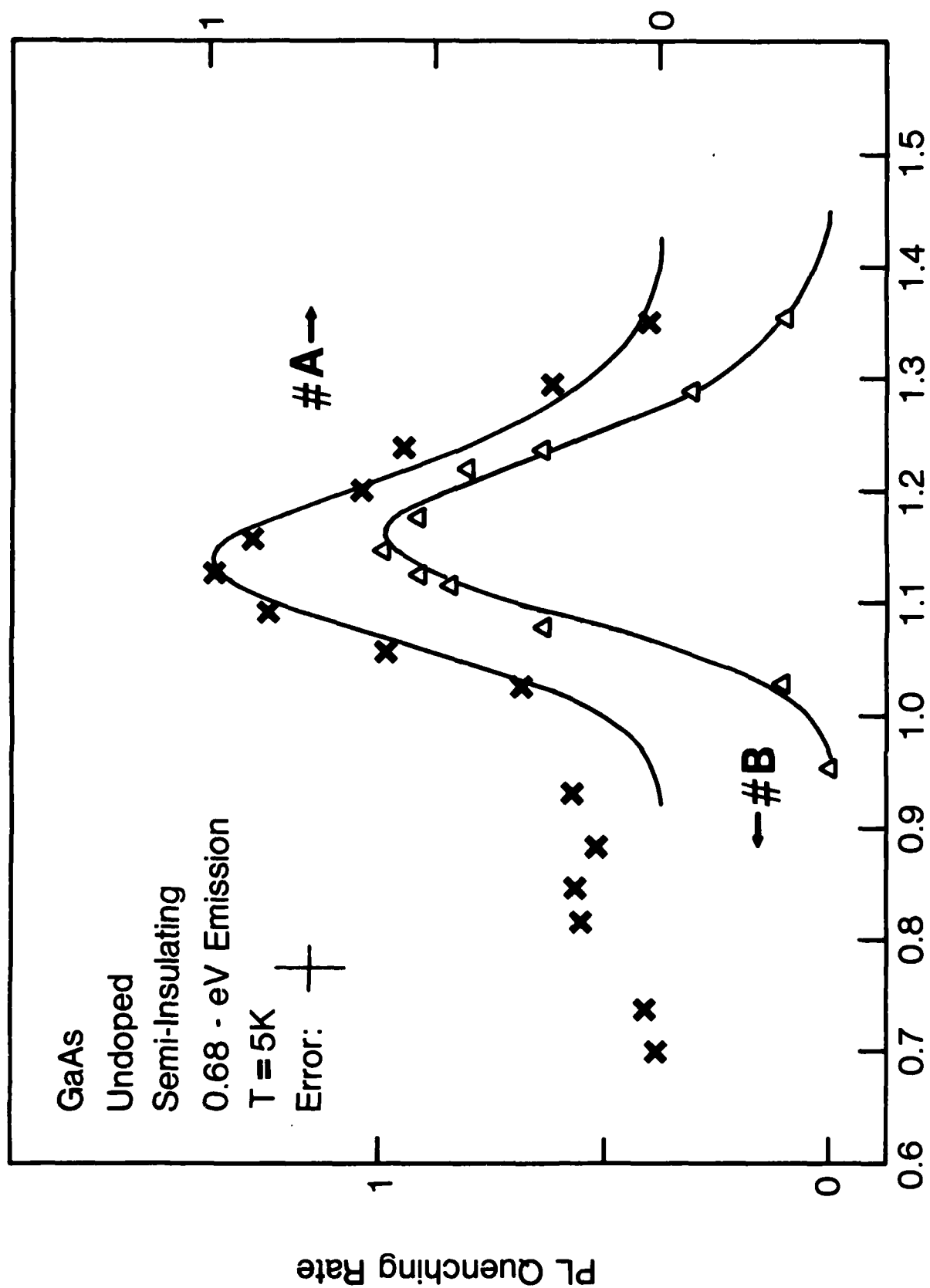
Fig. 3-4

0.68-eV band PL quenching rate vs. below-band-gap
excitation energy. Solid line is the representation of
a Gaussian curve.

21

source mass spectrometry indicates that incorporation of O into GaAs is difficult. A configuration diagram showing EL2 and O-related level is presented in Figure 3-5.

3.6 0.58-eV Emissions in Cr-doped Semi-Insulating GaAs (Ref.36)

Heat-treatment studies have been made on n-type conducting and semi-insulating GaAs crystals. Sharp zero-phonon lines at 0.598, 0.591, 0.584 and 0.576 eV and their phonon side-bands have been observed after heat treatment. It is found that the photoluminescence emissions are due to the presence of Cr. Close neighbour pairs involving Cr and other impurities are probably responsible for the emissions. Figure 3-6 shows the appearance of the 0.58-eV emission after heat treating at 600°C. The 0.584-eV zero-phonon line and its phonon side-band are seen clearly.
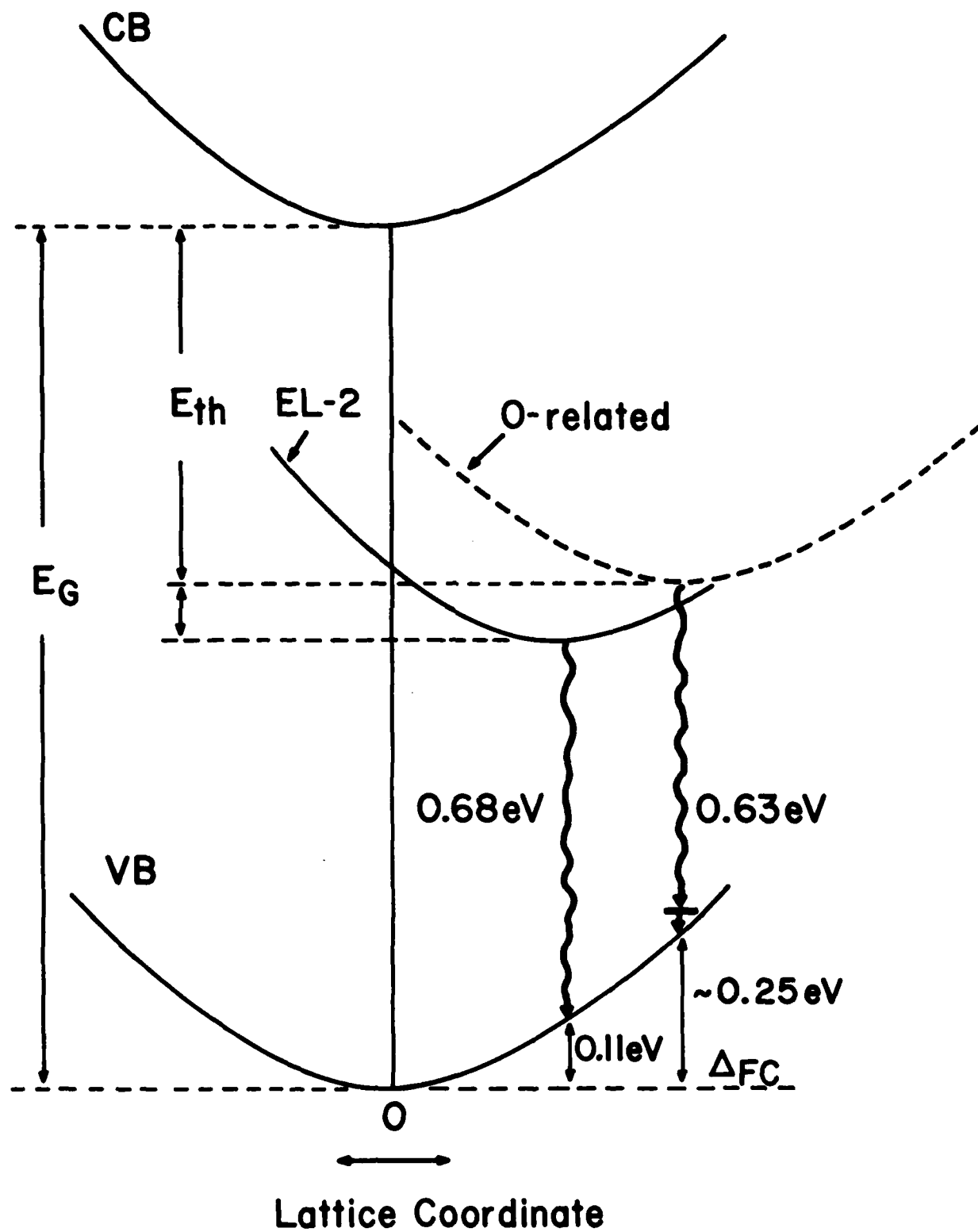
Fig. 3-5 Configuration diagram showing EL2 and O-related level.
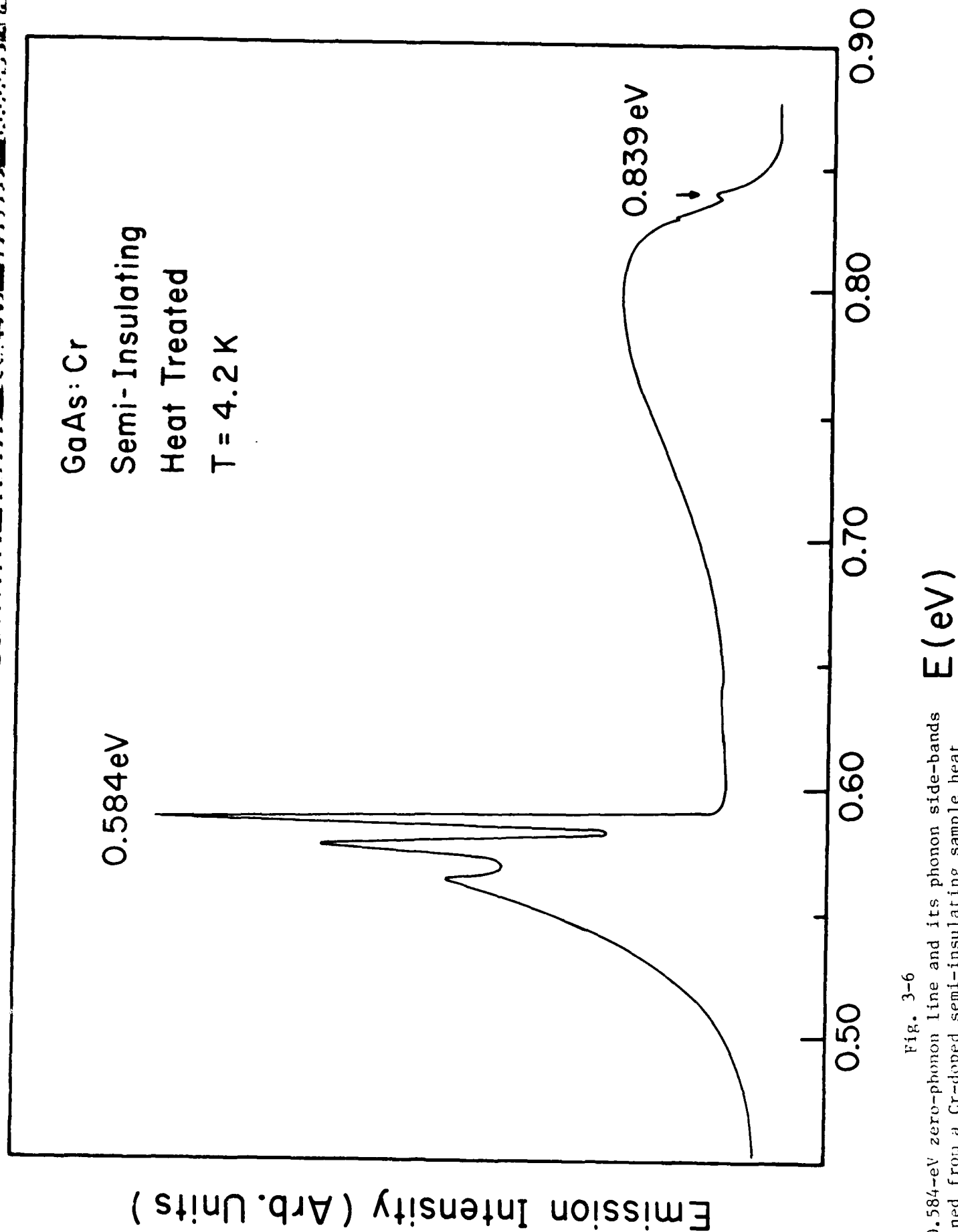
Fig. 3-6

The 0.584-eV zero-phonon line and its phonon side-bands obtained from a Cr-doped semi-insulating sample heat treated at 600°C.

24

4.0 PHOTOLUMINESCENCE IN CONDUCTING GALLIUM ARSENIDE AND INDIUM GALLIUM ARSENIDE

4.1 Introduction

The incorporation of an intrinsic defect has been known to produce electrically active centers in GaAs. In particular, many studies have been made on antisite defects formed during crystal growth[31, 37] and electron or neutron irradiation[38, 39]. The anion antisite double donor As_{Ga} or its complex has been explained to be responsible for a main electron trap located at ~0.75 eV from the conduction band (commonly known at EL2). The EL2 center is a main donor controlling electrical properties in semi-insulating substrate materials with the compensating effective-mass type shallow acceptor C_{As}, as discussed in Section 3. The concentration of EL2 increases with the As-melt composition. By using the same logic it can be expected that an acceptor can be produced by increasing the Ga-melt composition. This center is the cation antisite acceptor Ga_{As}. We have shown that such a center is present in p-type conducting and n-type semi-insulating GaAs. We will discuss the Ga_{As} center and some photoluminescence properties of epitaxial InGaAs crystals.

4.2 Temperature Dependence of 1.44-eV Emission in p-type GaAs (Ref. 40)

A study of the photoluminescence emission band at ~1.44 eV present in GaAs has been made at temperatures between 2-300 K. Changes in photoluminescence excitation intensity, emission energy, and emission intensity as a function of temperature lead to the identification of a 77 $\pm$ 2-meV deep acceptor. The temperature dependence of the emission-peak energy follows Eagles' model for the free electron-neutral acceptor transition. Figure 4-1 shows the temperature dependence of the 1.44-eV band.
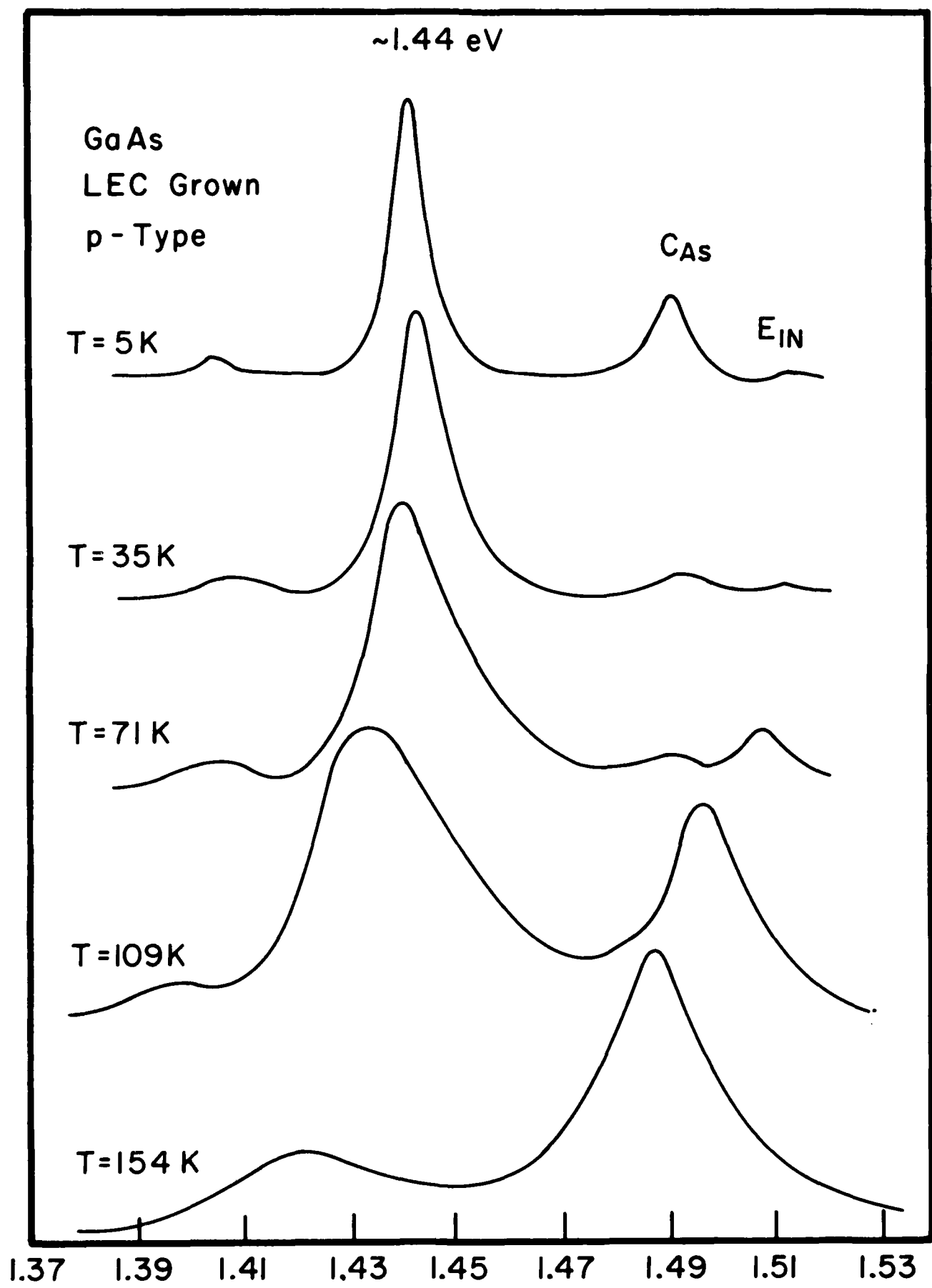
Fig. 4-1 Temperature dependence of the 1.44-eV band and the other emissions. "C_{As}" and "E_{In}" respectively mean the C_{As}-related and intrinsic-region emissions.

26

4.3 Energies of the Double Acceptor Ga_{As} in GaAs (Ref. 41)

Acceptors present in undoped p-type conducting GaAs have been studied with photoluminescence, temperature-dependent Hall measurements, deep level transient spectroscopy, and spark source mass spectrometry. It is shown that p-type conduction is due to the presence of the shallow acceptor C_{As} and the cation antisite double acceptor Ga_{As}. The first and second ionization energies determined for Ga_{As} are 77 and 230 meV from the valence-band edge. Figure $^{4-2}$ contains the 4.2-K photoluminescence bands showing the first and second ionization levels of the Ga_{As}.

4.4 Photoluminescence Excitation of the 1.44-eV Emission in p-type GaAs (Ref. 42)

Photoluminescence excitation spectra have been obtained at 4.2 K for the 1.441-eV cation antisite double acceptor Ga_{As} emission present in undoped p-type GaAs. The oscillating structures at above-band-gap energy can be attributed to the energy relaxation of the conduction-band electron by the successive emissions of the zone-center longitudinal phonon. The energy of the oscillatory periods shows that the 1.441-eV emission at 4.2 K is primarily due to the neutral donor-acceptor pair transition involving the Ga_{As} center. Figure 4-3 shows the photoluminescence excitation spectra obtained from two samples.

4.5 Photoluminescence of Mn- and Un-doped $Ga_{0.47}In_{0.53}As$ on InP (Ref. 43)

Photoluminescence measurements on Mn- and Un-doped liquid phase epitaxy $Ga_{0.47}In_{0.53}As$ on InP have been made at the temperature range of 4.2-296K. The Mn acceptor binding energy is estimated to be 45 ± 2 meV. Luminescence due to the Mn acceptor quenches at 60-100K depending on the doping concentration of Mn in favor of a near-band edge emission. Figure 4-4 shows the 4.2-K photoluminescence in undoped and Mn-doped $In_{0.53}Ga_{0.47}As$.

27
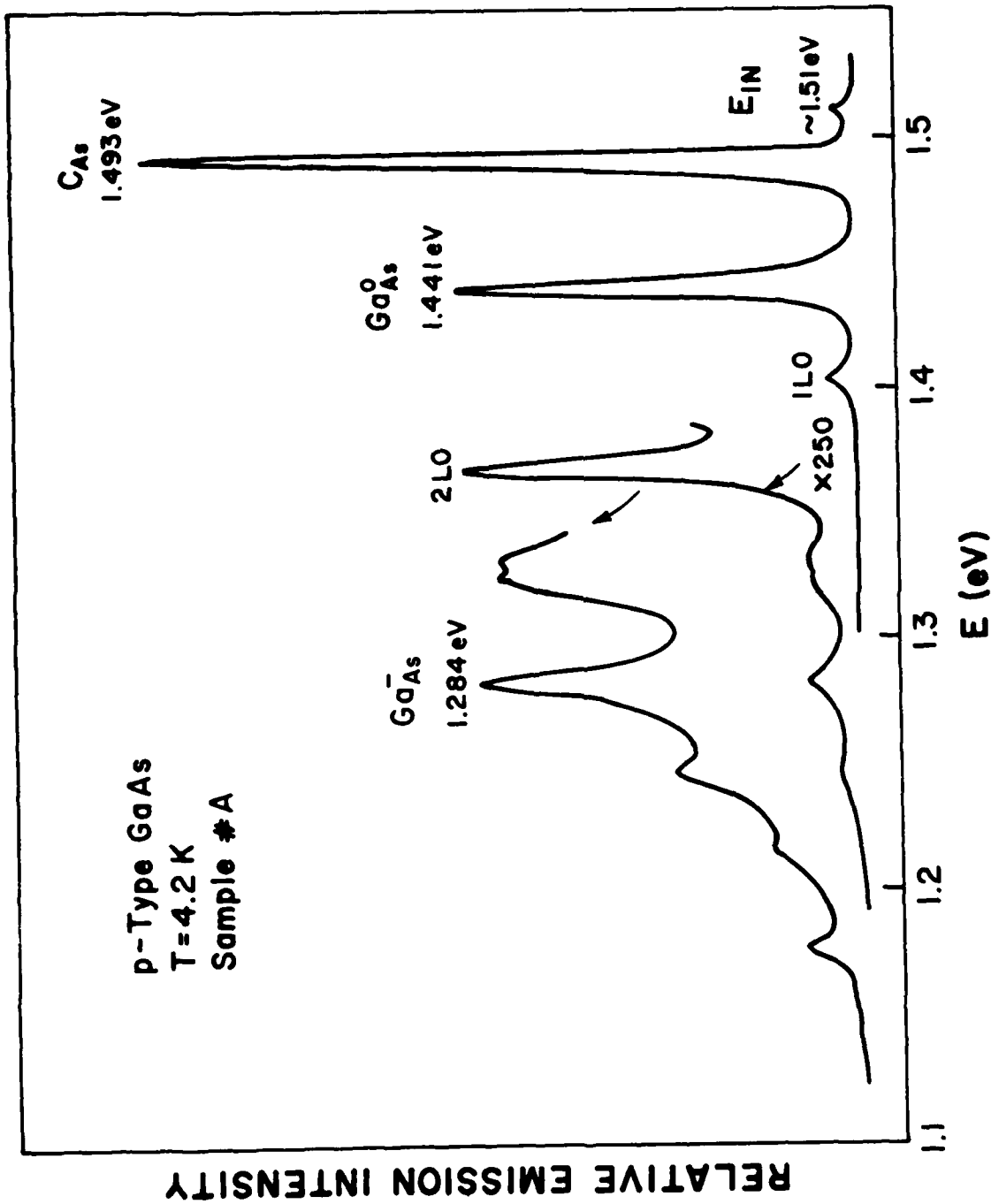
Fig. 4-2 T = 4.2-K photoluminescence characteristics of a p-type sample. The near-intrinsic region (E_{In}), C_{As}-related emission at 1.493 eV, and the emissions at 1.441 and 1.284 eV due to Ga_{As}^0 and Ga_{As}^-, respectively, are seen.

28
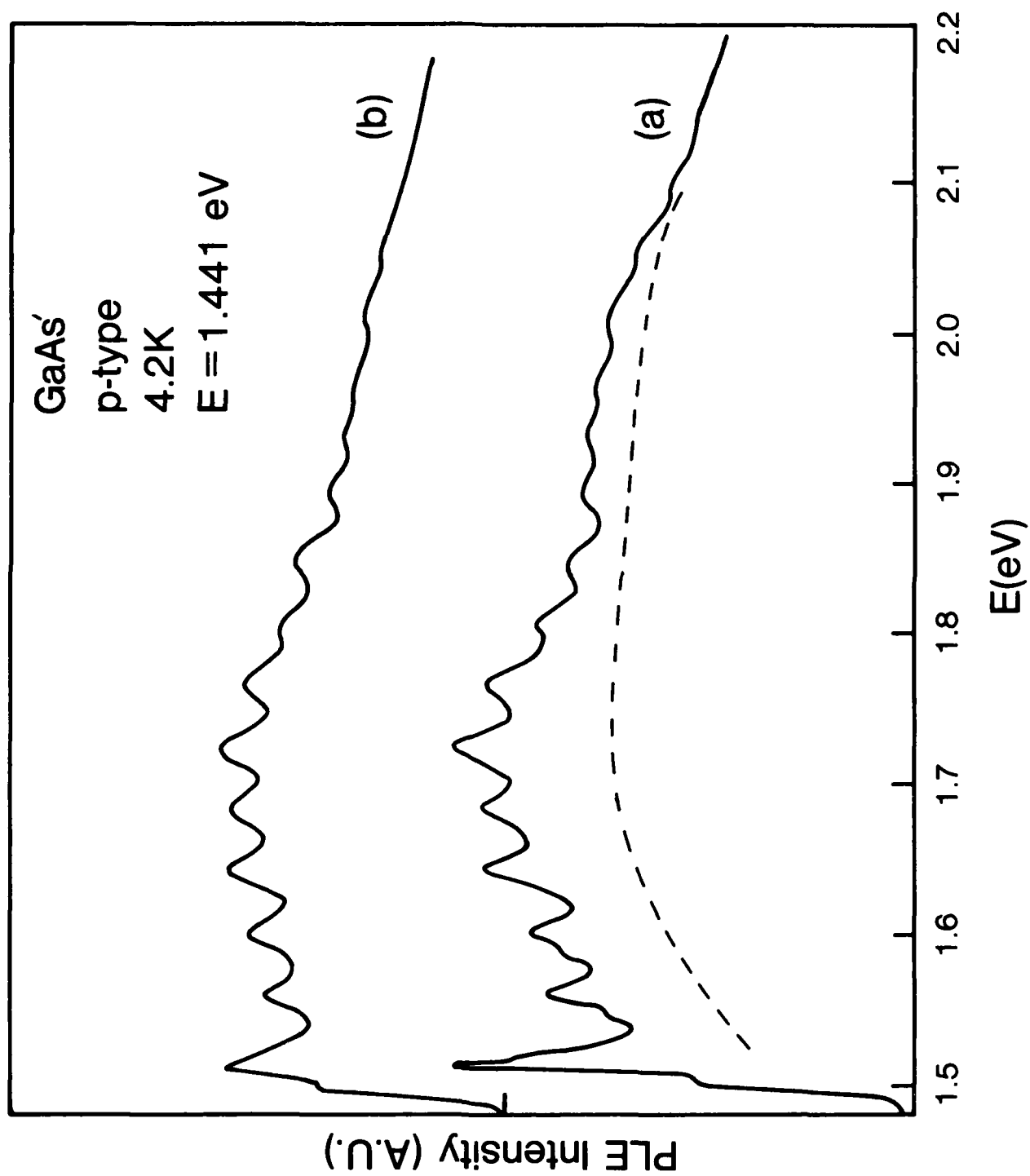
Fig. 4-3 Photoluminescence excitation spectra obtained from two p-type samples.

29
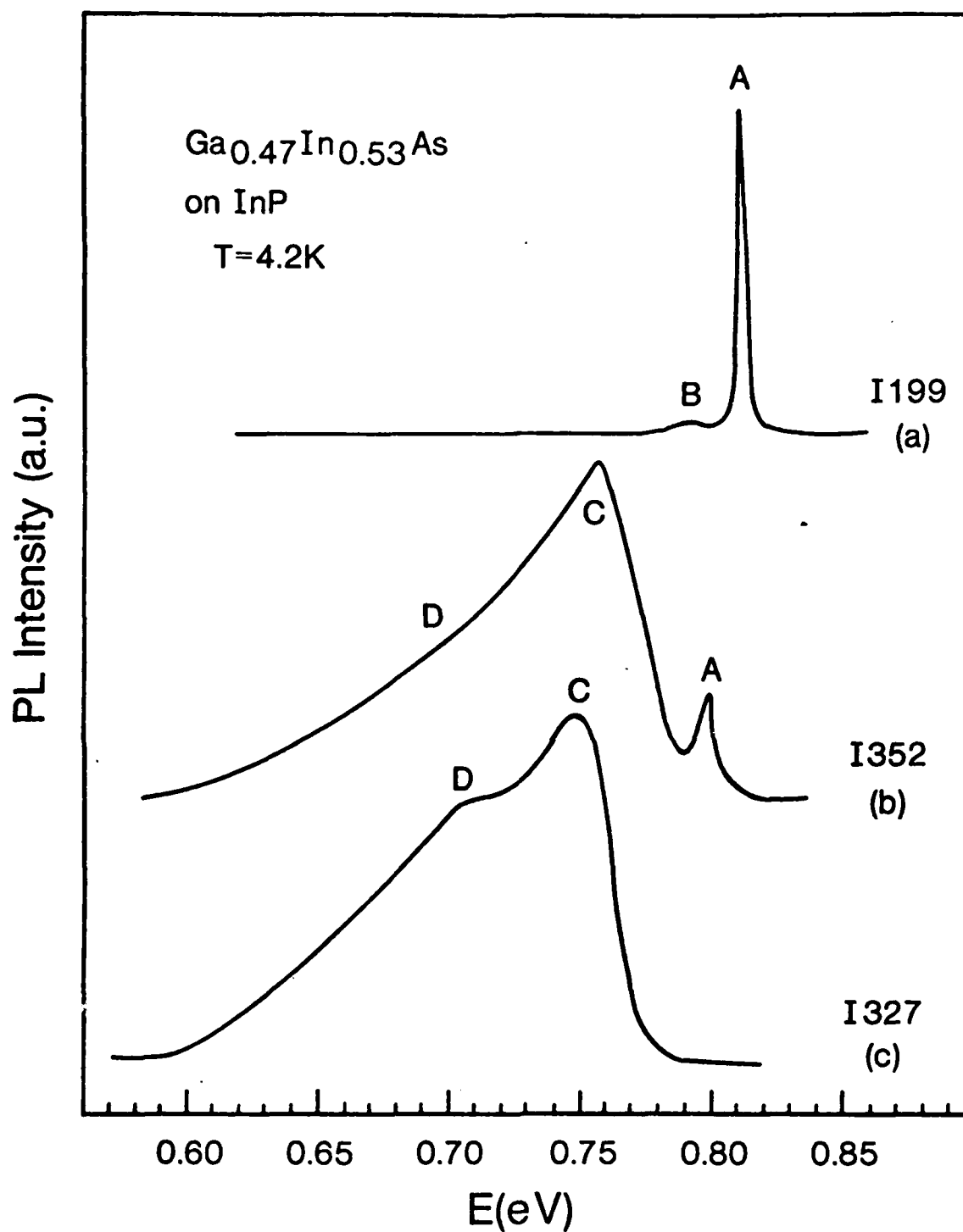
Fig. 4-4   4.2-K photoluminescence spectra obtained from (a) undoped
n-type samples, (b) lightly Mn-doped p-type, and (c)
heavily Mn-doped p-type samples.

5.0 LOCAL VIBRATIONAL MODE IMPURITY STUDIES IN GALLIUM ARSENIDE

Impurity analysis of semiconductor materials such as GaAs may be accomplished with quantitative accuracy and sensitivity by use of infrared techniques. Impurities whose atomic masses are smaller than those of the host semiconductor induce a localized vibrational mode (LVM) absorption which may be detected in infrared transmission. One important aspect of such measurements is that the location in the lattice (i.e., being substitutional on either an As or Ga site) will cause frequency shifts of the LVM. In addition, this technique is nondestructive and does not depend on any particular electrical activation of the impurity for it to be measured.

The main thrust of the investigation has involved high resolution measurements of the LVM due to carbon and silicon in GaAs. A rapid scan Fourier Transform Infrared spectrometer was operated at the highest attainable resolution of 0.06 cm^{-1} with the sample held at 80 K in a cryostat equipped with CdTe windows. A helium cooled bolometer (nitrogen cooled HgCdTe detector) with mylar (germanium) beamsplitter was used for the silicon (carbon) LVM measurements. Samples with carbon concentrations [C] between 4 x 10^{15}/cm^3 to 1 x 10^{17}/cm^3 and [Si] between 1 x 10^{18}/cm^3 to 5 x 10^{19}/cm^3 were found to have additional structure as compared to previous low resolution measurements. On the basis of these measurements, direct evidence for the site of substitutional carbon in GaAs as being on the As sublattice was obtained.[44]

The cause of the splittings of the LVM absorptions for impurities on the As sublattice are the various configurations of the isotopes of nearest neighbor, nn, Ga isotopes. Using the relative natural abundance of the Ga isotopes of masses 69 and 71 which are 60.4% and 39.6%, respectively, and the statistics of the possible configurations for the four nn

31

Ga isotopes, it was possible to use a linear chain model (neglecting bond bending) to predict the relative heights of the individual lines. Due to several near degeneracies, the predicted heights (assuming equal oscillator strengths for each) were 1.00, 0.35, 0.24, and 0.50 whereas measured strengths in carbon doped samples was 1.00, 0.4, 0.3, and 0.5 where in each case normalization was to the highest energy or all ^{69}Ga isotope nn case. Furthermore, the frequency shift when all nn are of ^{69}Ga to that of all ^{71}Ga may be calculated by

$$\frac{\omega_1}{\omega_4} = \left(\frac{M_1}{M_2}\right) \frac{2M_2 - M_{c,Si}}{2M_1 - M_{c,Si}}$$

which yields 1.0013 for ^{12}C and 1.0036 for ^{28}Si as compared to the measured value of 1.00083 and 1.0028 for these impurities. A typical spectrum for carbon-doped GaAs is shown in Figure 5-1. This particular sample was analyzed by Spark Source Mass Spectroscopy to have $[C] = 1.3 \times 10^{17}/cm^3$ and by Secondary Ion Mass Spectroscopy to have $[C] = 1 \times 10^{17}/cm^3$ which yields a calibration factor[45] of 1 cm^{-2} absorption corresponding to a $[C]$ of $3.6 \times 10^{16}/cm^3$.

One of the most important features of this entire study is the unambiguous determination of the site for carbon in GaAs. Since carbon and silicon can occupy either Ga or As sites, with consequent donor or acceptor electrical characteristics, this is of some technological inter-est. In previous studies[46] the LVM absorption due to Si$_{Ga}$ was identified to occur at 384 cm^{-1} and that due to Si$_{As}$ at 399 cm^{-1}. Such lines were measured in the high resolution condition to yield the results shown in Figure 5-2. The lineshape of the Si$_{As}$ is extremely similar to that of carbon at 582 cm^{-1} which suggests that carbon occupies the As site and that the theoretical explanation is correct. No line could be identified
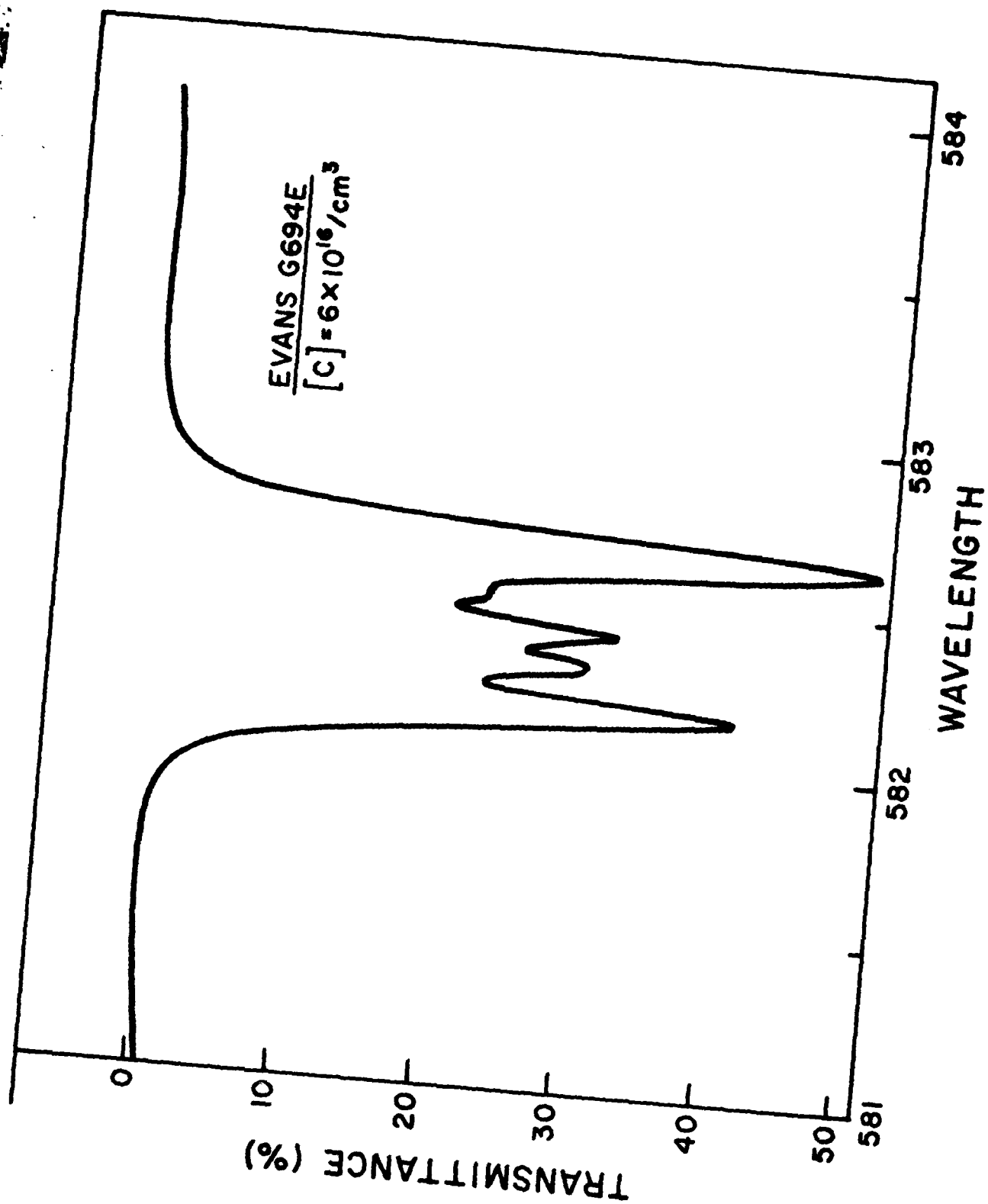
Fig. 5-1 High resolution infrared transmission spectrum of carbon doped GaAs.

33
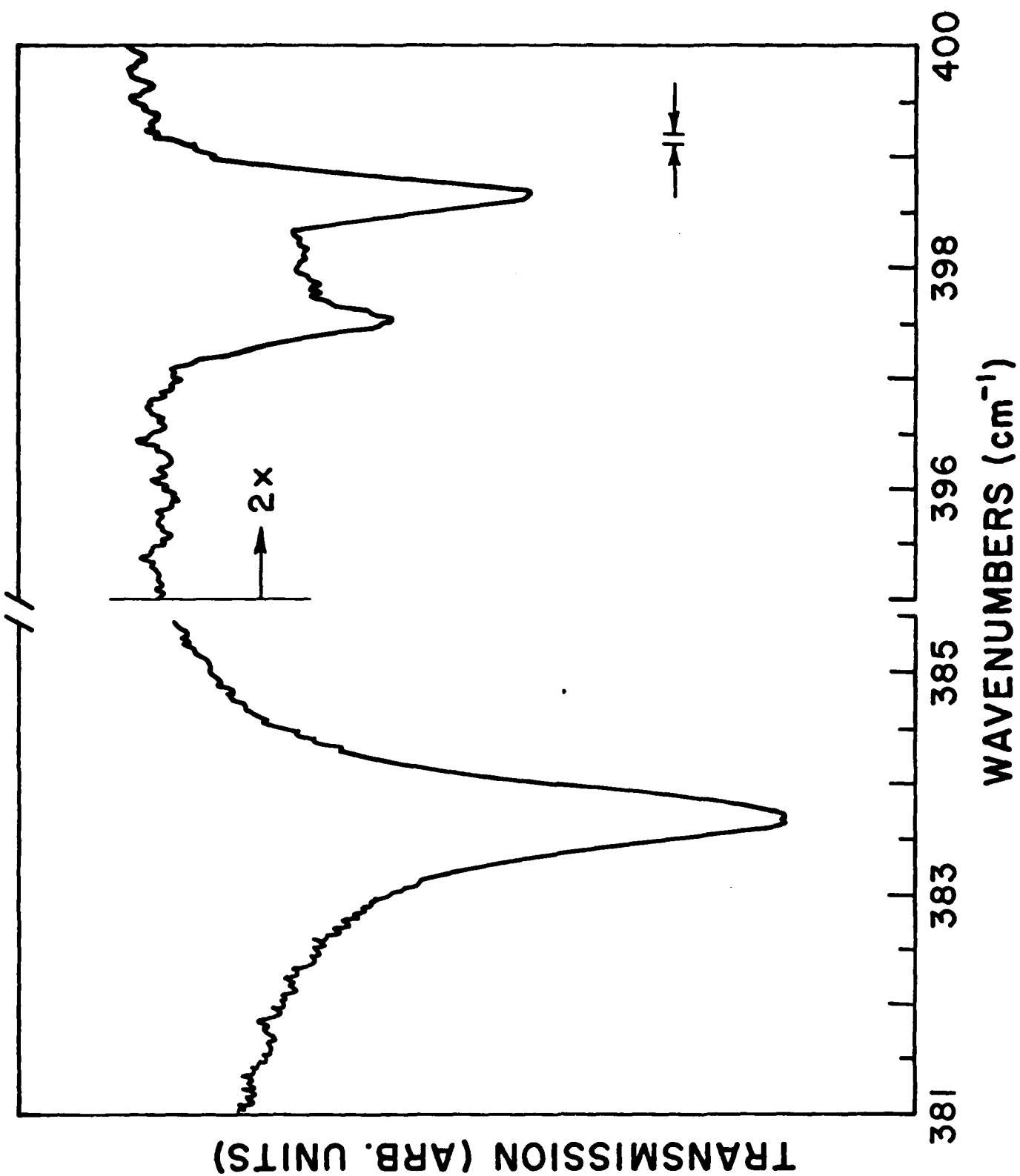
Fig. 5-2 High resolution infrared transmission spectrum of silicon-doped GaAs.

34

in carbon-doped samples which would correspond to C_{Ga} although the $^{13}C_{As}$ line was observed. Since ^{13}C is only 1% abundant, the C_{Ga} must be less than this, if it exists at all. This is to be contrasted with the behavior of Si in GaAs, which prefers the Ga site by two orders of magnitude over the As site. Several theoretical calculations have now been performed which support the conclusions drawn by the simple linear chain model. Second order degenerate perturbation theory[47] and Green's function[48] techniques also fit the data well and yield important lattice constant information.

Additional features in Si heavily-doped GaAs were also studied in some detail. For example, Si_{Ga}-Si_{As} pair modes should also show the effects of nn Ga isotopes. Since in this case, the symmetry is lower (C_{3v}) and there are only three Ga neighbors to the Si_{As} in the Si-Si pair, the lineshapes are expected to differ from the previous cases. The high frequency mode (A_1^+), being singly degenerate splits into four lines whose widths are unfortunately less than the spacing and hence result in an asymetric lineshape. The low frequency mode at 393 cm^{-1} is doubly degenerate (E^+) which causes some split lines to become degenerate. Again, the result predicted by a linear chain model can be made to fit the observed asymmetric lineshape assuming only that individual modes are of typical widths as other lines in the sample (0.7 cm^{-1}) with the only adjustable parameter being the spacing between lines. Although the fit is not unique, a spacing of 0.4 cm^{-1} appears correct. A Green's function calculation has been done for the Si-Si pairs[49] which shows essentially the observed behavior. Finally, in a sample doped both with ^{30}Si and ^{28}Si, the modes were resolved corresponding to $^{28}Si_{Ga}$-$^{30}Si_{As}$ and

35

$^{30}Si_{Ga}$-$^{28}Si_{As}$ to be at 455.80 and 457.01 cm^{-1}, respectively, which is again a very sensitive measure of lattice spring constants.

In Si-doped GaAs which was compensated by either ^{6}Li or ^{7}Li diffusion, the isolated Li_{Ga} line was seen for the first time, although it had been sought previously by other groups. This mode occurs at 449.64 cm^{-1} for $^{7}Li_{Ga}$, which is near the energy which might be predicted from the ^{7}Li absorption in a Si_{Ga}-Li_{Ga} pair, when the formula

$$\overline{\nu}^2 = \frac{1}{3} \sum_{i=1}^{3} \frac{\nu}{\nu_i^2}$$

is used with the observed position of 454.19, 447.39, and 437.75 cm^{-1} or a predicted value of 446.49 cm^{-1}. A similar result for ^{6}Li is obtained with the observed $^{6}Li_{Ga}$ occurring at 482.31 cm^{-1}. Examples of such samples may be found in Figure 5-3.

In Si-doped GaAs which was compensated with electron irradiation, additional structure was observed between 365-376 cm^{-1}. One line in particular, 366.63 cm^{-1}, has been attributed to Si_{As} paired with an nn defect on the Ga lattice such as the Ga vacancy or As_{Ga} antisite[50]. The large width of the line suggests Si_{As} involvement. Also, the defect appears to have a donor activation and appears in both electron-irradiated and Li-compensated samples. Previous studies[51] indicate that the line diminishes with increased electron irradiation and grows upon annealing. The most probable candidate fitting these observations is Si_{As}-As_{Ga} and is line "A" in Figure 5-3. The origin of lines "B" - "E" is undetermined although closely associated with the electron irradiations. An additional important conclusion when comparing samples compensated by either method is that in high resolution neither the position nor widths of any line were different between the two compensation methods. It is well known, however, that amplitude will vary due to impurity redistribution. This important result
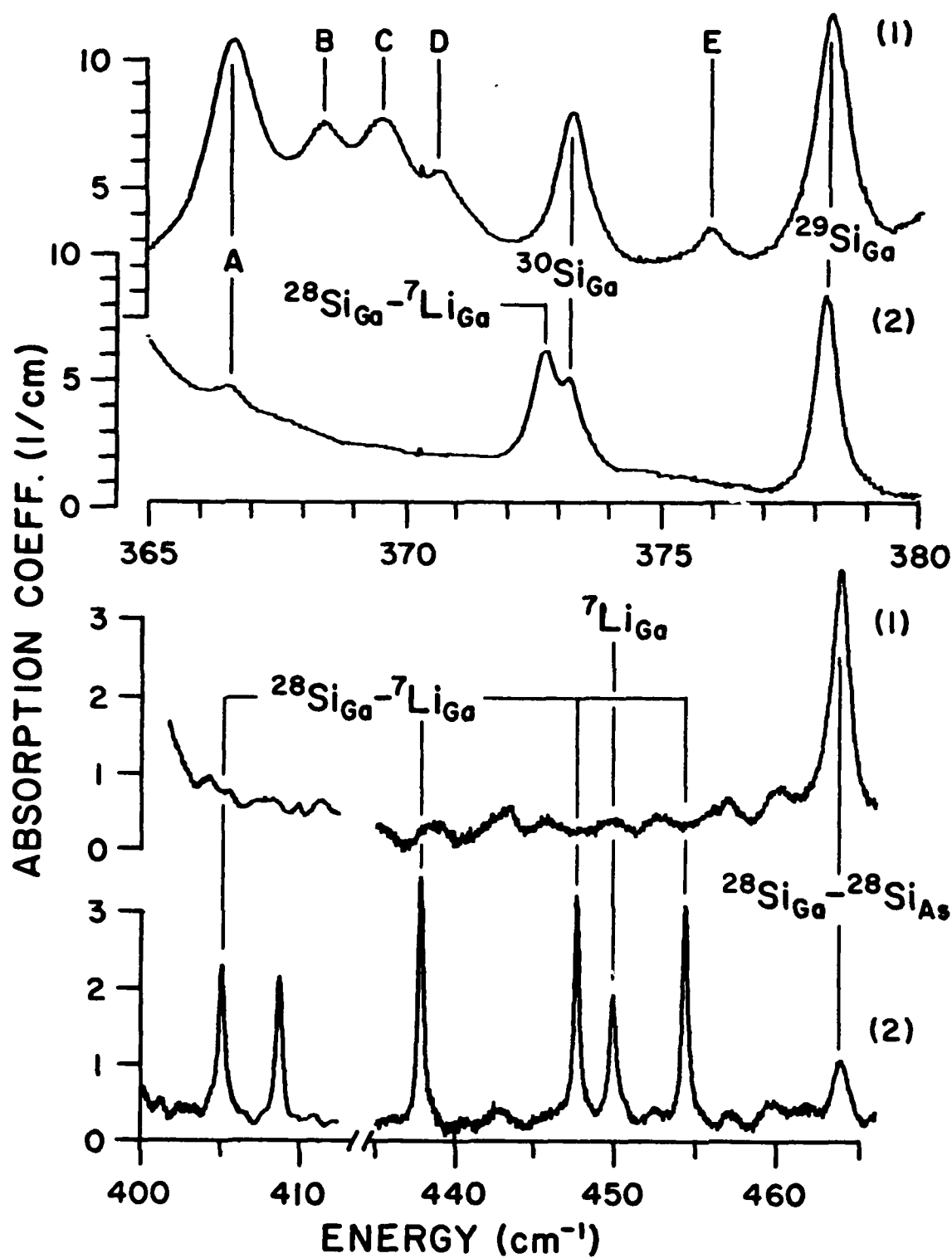
Fig. 5-3   High resolution infrared absorption spectra for
two silicon-doped GaAs samples. Sample 1 was
compensated by electron irradiation while
Sample 2 was compensated by Li diffusion.

37

verifies that samples may be studied using either means of compensation
without perturbation due to the presence of Li. Additional unidentified
absorptions were also investigated but no conclusive evidence for an
identification was obtained.

38

6.0   I-V CHARACTERISTICS OF GaAs JFET's

6.1   Introduction

Since the junction field-effect transistor (JFET) is one of the most important devices made of semiconductor materials and the current-voltage (I-V) characteristics are the basic tool to study the performance of such devices, it is very important to study and understand the quantitative dependence of the I-V properties on the basic material parameters obtained mainly from electrical characterization. Carrier drift velocity as a function of the electric field (V-E) in the conducting channel of the device is introduced as an input in the calculation of the I-V characteristics. Previous models use a V-E curve which is either linear[52] or gradually changes from the low-field range of constant mobility to a saturation value[53]. The latter V-E relationship represents correctly the behavior in semiconductors like Si or Ge. However, for some semiconductors with two conduction-band valleys, e.g., GaAs and InP, the velocity-versus-field curve has a peak, and a so-called negative conductance region, in which the drift velocity decreases with increasing field. We have shown[54] that a large difference occurs in the I-V characteristics and saturation current, especially for small gate voltages, if one takes into account the realistic field-dependent velocity for GaAs. In the next section we briefly describe the model. A detailed discussion may be found in Ref. 54.

6.2   Theoretical Model for JFET

Lehovec and Zuleeg used the Trofimenkoff-type velocity-field relationship in their model

$$v = \frac{\mu E}{1 + \mu E/v_m} \quad . \tag{6-1}$$

39

Kroemer[55] introduced the following velocity-field characteristic

$$v = \mu E \left[\frac{1 + (AE)^k}{1 + (AE)^k \mu E / v_m} \right] .$$ (6-2)

At high fields, v approaches a saturation velocity, v_m and at low fields, the velocity is linear in E with a low-field mobility μ. A peak occurs in the intermediate region. This expression gives a good fit to the measured velocity[56] as shown in Figure 6-1, where we have assumed the saturation velocity to be 1.14×10^7 cm/sec and the low-field mobility to be 7500 cm^2-V/sec[6]. The values of the two fitting parameters are: $A^{-1} = 5.2$ kV/cm and $k = 4.2$. In the same figure, we have also shown the Trofimenkoff v-E curve (Eq. 6-1) with the same values of low-field mobility μ and the saturation velocity v_m. We then obtain the I-V characteristics using the field-dependent velocity given by Eq. 6-2 and with the other approximations similar to those used by Shockley[52].

Current is proportional to the drift velocity v and the open channel thickness (a-d), where a and d are the total channel and depletion thicknesses, respectively. Since the Poisson's equation relates this d to the potential at that point and v is a function of the field, which is just the derivative of the potential, we obtain a differential equation for the potential V, with the current as a parameter in the equation. Solving the differential equation into proper boundary conditions, namely,

$$x = 0, \quad y = t \equiv (-V_{GB}/V_o)^{\frac{1}{2}}$$

$$x = L, \quad y = u \equiv [(V_D - V_{GB}/V_o]^{\frac{1}{2}} ,$$ (6-3)

where V_{GB} is the sum of the gate voltage and the built-in voltage, V_D, is
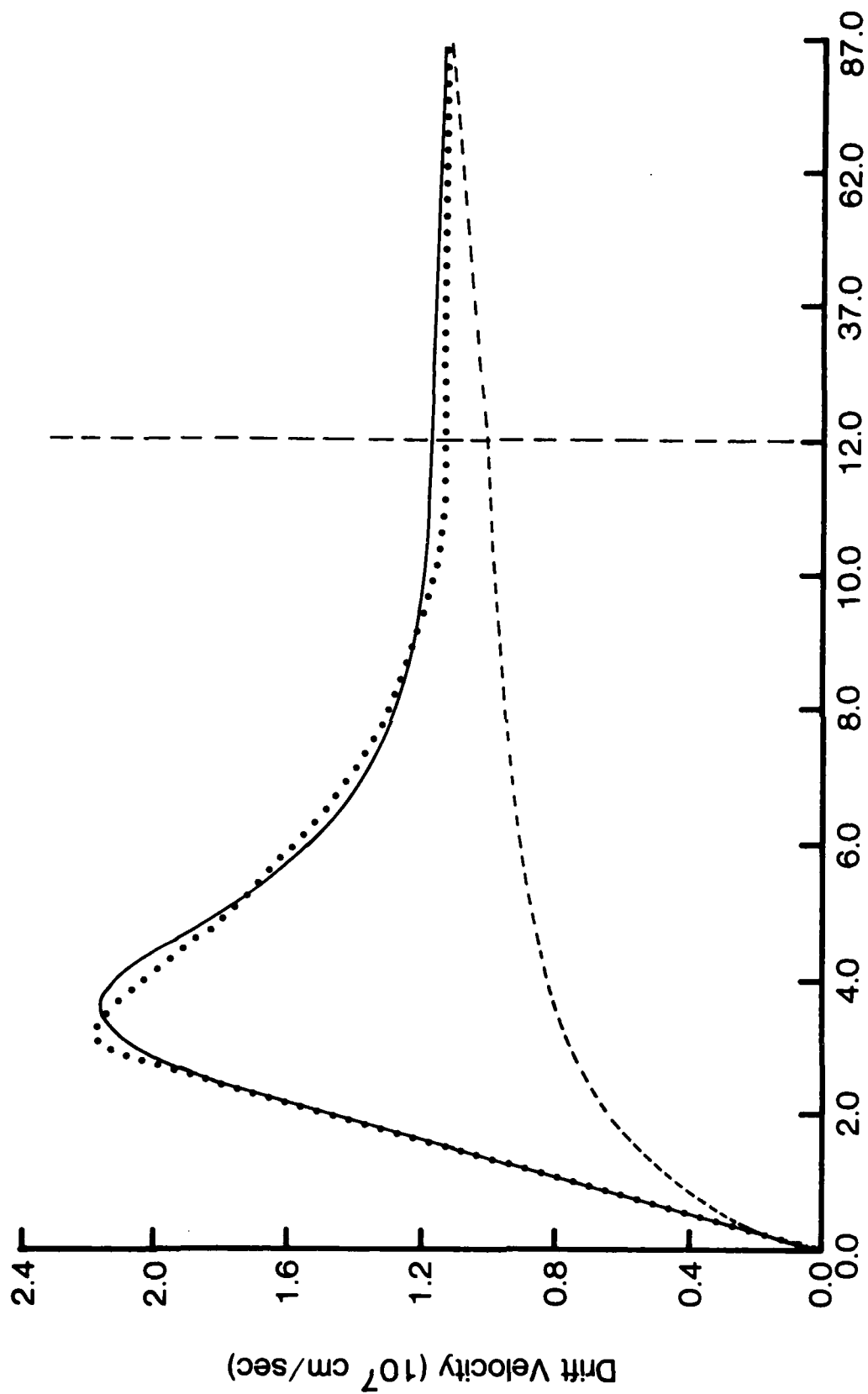
Electric Field (KV/CM)

Fig. 6-1 Drift velocity versus electric field. Dotted line represents experimental values; solid line represents Kroemer's analytic expression; and the dashed line is from Trofimenkoff's expression. Note the scale change in the field axis.

41

the applied drain voltage, $x = 0$ and L are the positions of the source and drain, respectively, and V_o is a parameter (which depends on impurity density in the channel and the total channel thickness) we obtain an implicit equation for the current as a function of V_D, V_G and their material and device parameters. With the V-E relationship given by Eq. 6-2, it is not possible to solve this equation analytically, although its numerical solution is simple. Figure 6-2 shows the numerical solution for the reduced current β with the reduced gate voltage t as a parameter (solid curves). The dashed curves are plots of the results of Lehovec and Zuleeg[53] corresponding to the velocity characteristics represented by the dashed line in Figure 6-1. In all of the figures solid lines are referred to as CL and dashed ones as LZ. The various parameters used in our calculations are: $N = 3 \times 10^{15} cm^{-3}$, $W = 1.25$ mm, $a = 1.4$ μm, $L = 25$ μm, $\varepsilon = 12.9$. These are the parameters for the Device PN-1-S of Lehovec and Zuleeg[53]. Conclusions drawn in this paper also hold for devices with more realistic parameters for GaAs FET's. For a better understanding of the reasons for the large difference in the I-V curves (solid and dashed) we have computed the open channel thickness (i.e., the shape) and the field along the channel and have plotted these quantities in Figures 6-3 and 6-4, respectively. We have plotted in Figure 6-5 the transconductance g_m (in units of the transconductance g_{mo} for the Shockley model (i.e., linear v-E relationship) versus the reduced gate voltage $-V_{GB}/V_o$. The transconductance obtained by Lehovec and Zuleeg[53] does not agree with that of the present calculation. This shows that the CL saturation currents for various gate voltages cannot be obtained by a simple scaling from those of LZ.
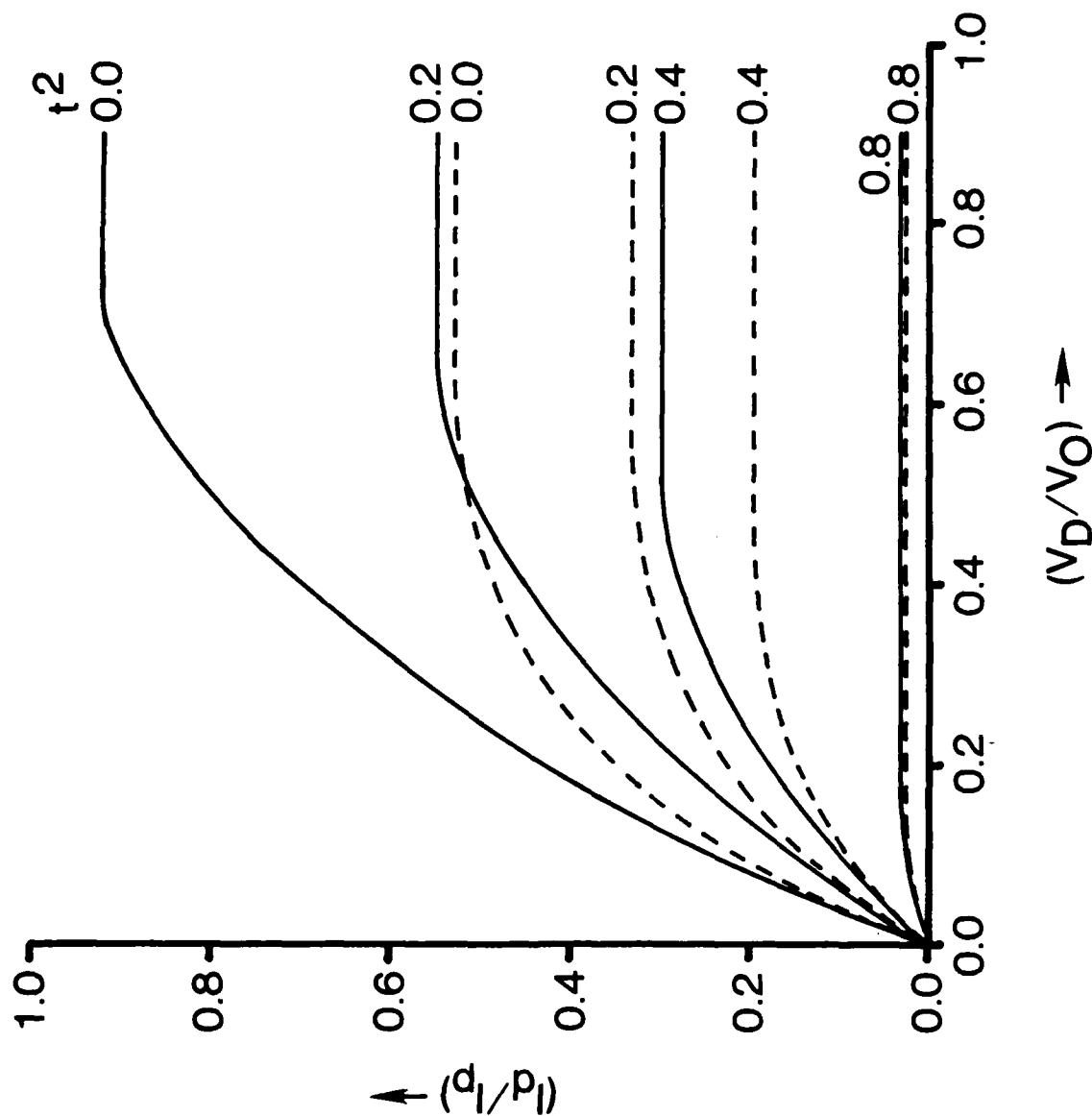
Fig. 6-2 Reduced drain current versus reduced drain voltage with the reduced gate voltage, $t^2(= -V_{GB}/V_O)$ as a parameter. In this figure as well as those following, solid lines are from the present calculation and dashed lines are due to Lehovec and Zuleeg.

43

	t^2	V_D/V_O
1(a)	0.0	0.2
1(b)	0.0	0.9
2(a)	0.4	0.2
2(b)	0.4	0.9

1(a)

1(b)

2(a)

2(b)

Position in the Channel x/L

$(1-d/a)$ →
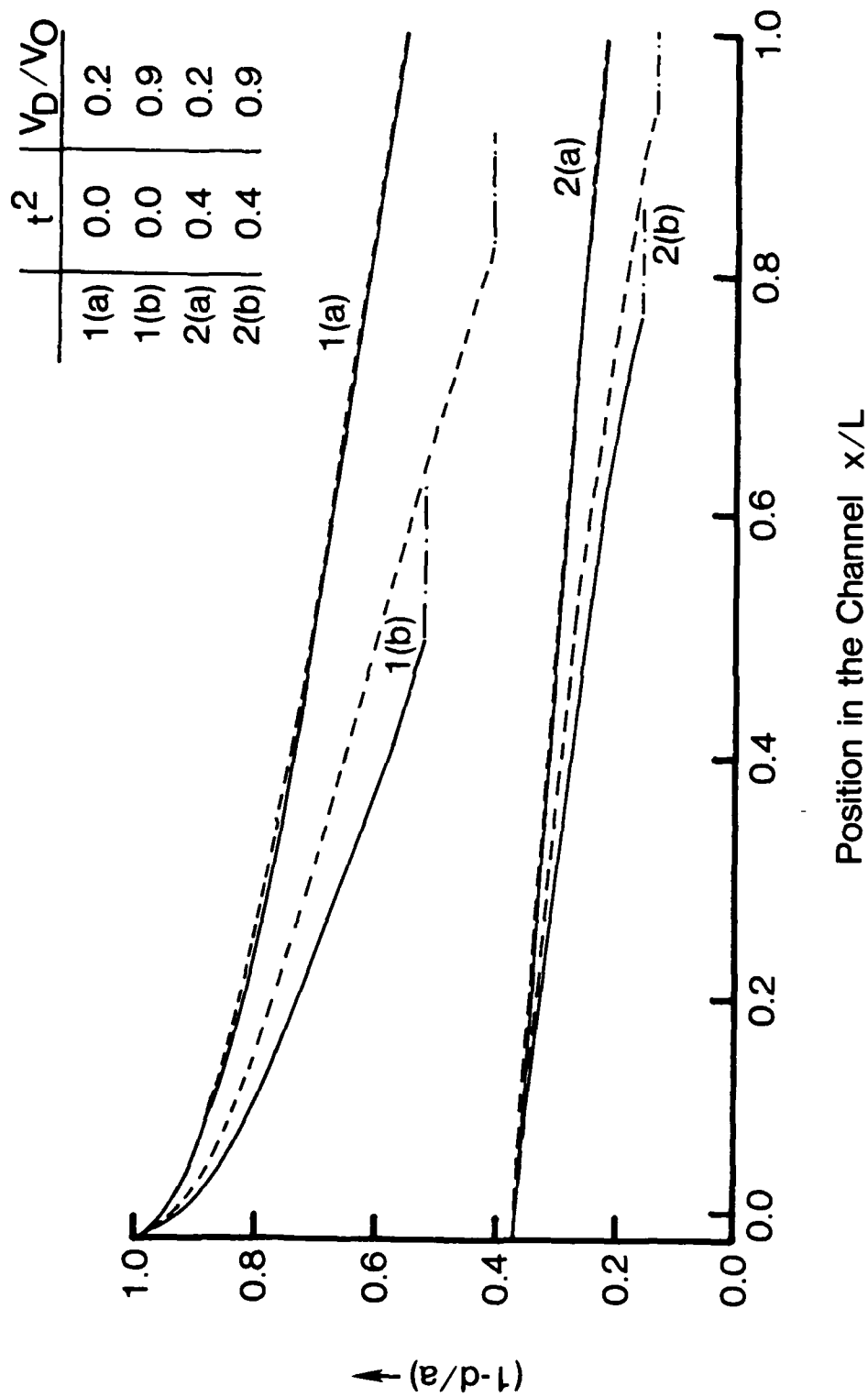
Fig. 6-3 Fractional thickness of the open channel, as a function of position, for the parameters shown.
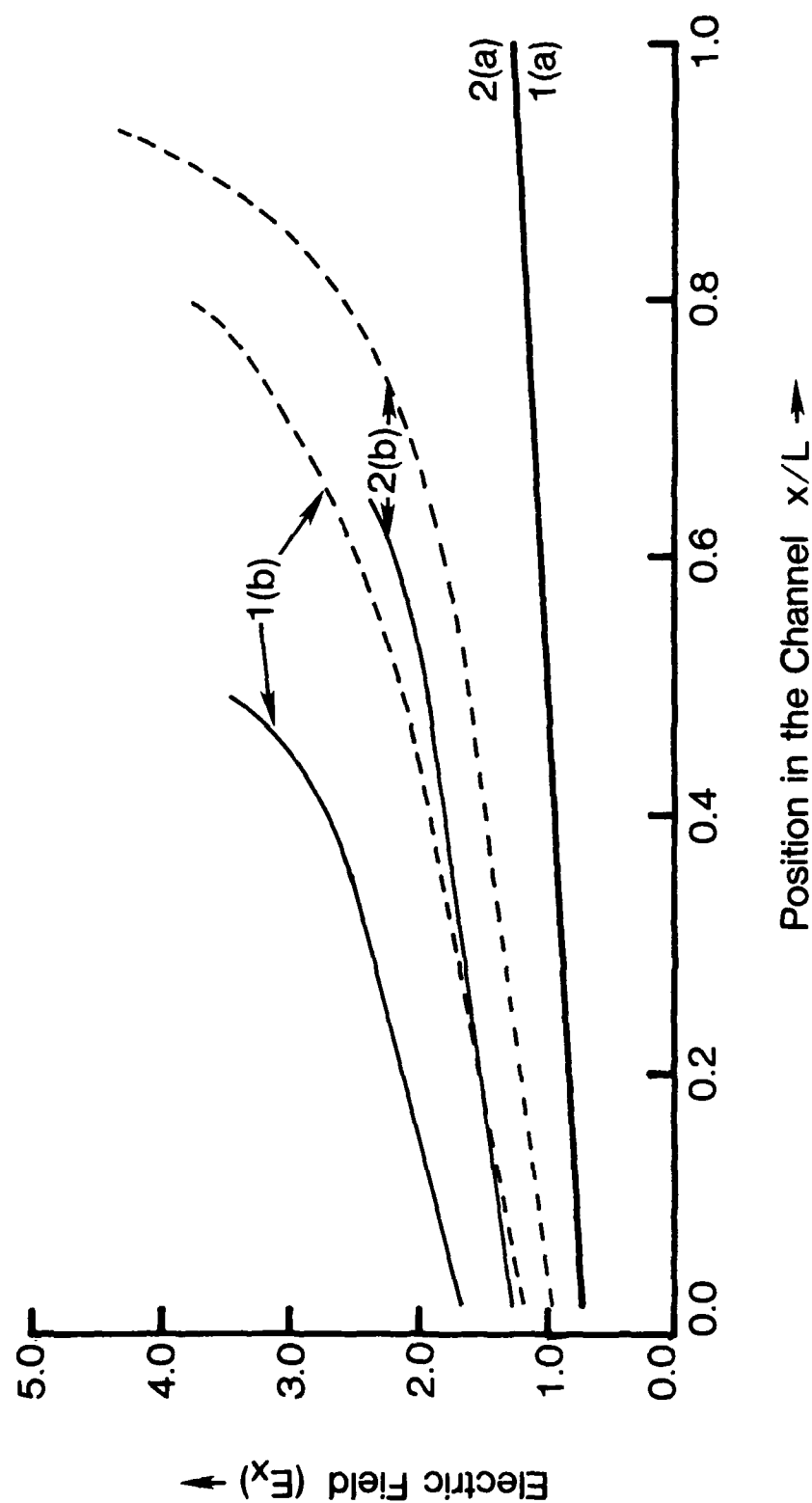
Fig. 6-4 Electric fields along the channel for the same set of parameters as in Fig. 6-3.

45
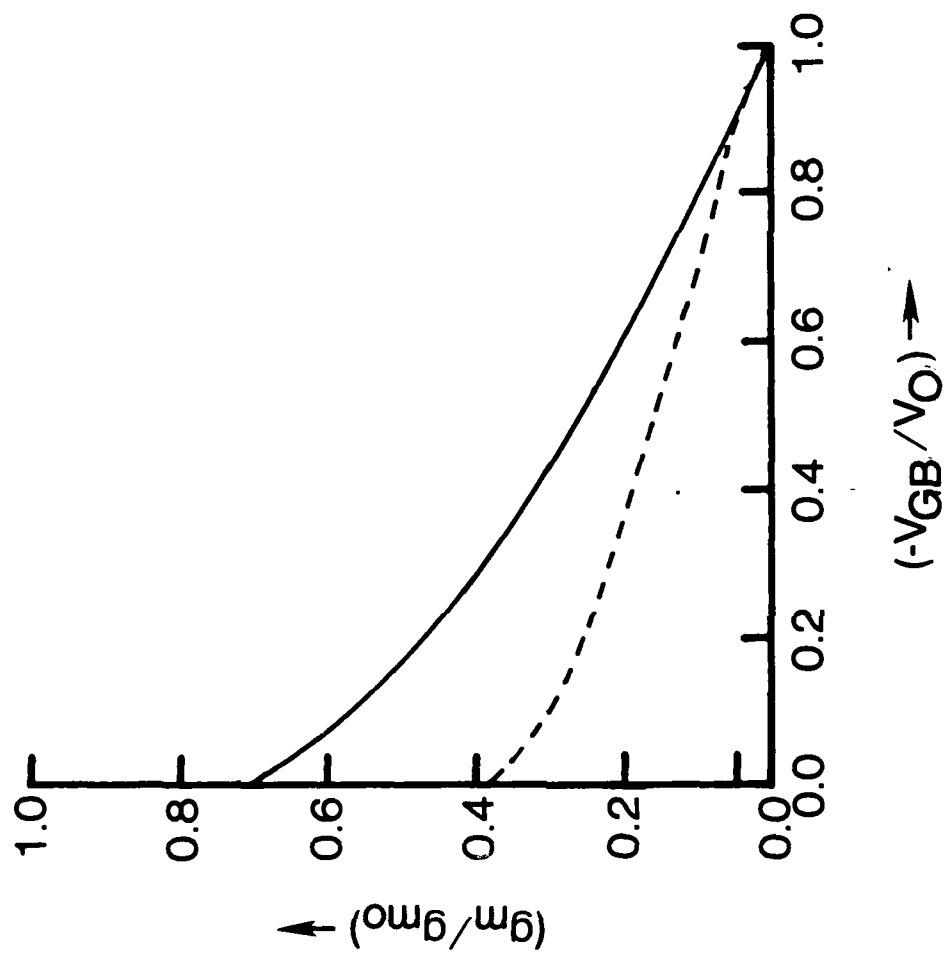
Fig. 6-5 Reduced transconductance versus reduced gate
voltage.

46

6.3 Physical Parameters of FET's

In the model described in Section 6-2, we have fitted the experimental V-E data of Smith, et al.[56] with Eq. 6-2. This set of data is for a pure sample, whose low-field mobility (μ_L) is 7500 cm^2/V-sec. However, the conducting channel region of an actual device has lower μ_L. The main reason for this low μ_L is that impurities are incorporated in the region to provide the carriers for the device operation. Scattering of the carriers from the ionized impurities reduces the mobility at lower fields. Since the Coulomb scattering cross section is inversely proportional to the fourth power of the velocity of the incident particle, the V-E curve is not expected to be much different at higher fields. Therefore, in the absence of measured V-E curve for the channel material, we need to modify the V-E relationshp (Eq. 6-2) such that it gives μ_L equal to the measured value ($\sim$4000 cm^2/V-sec), but it remains the same in the high field region. To achieve this, we add an emperical term ($\propto E^2$) such that the peak in V-E remains the same. We have developed an efficient computer program to fit the measured I-V data with the calculated I-V data, and the best fit provides the geometrical and material parameters. The model calculation includes the aforementioned modified V-E relationship. It may be noted that if a more reliable V-E relationship, either measured or theoretically calculated, is available, we would be able to incorporate it fairly simply.

The following are the parameter values for the device COM 130S87 obtained by fitting the I-V data (measured in this laboratory) with our model (See Figure 6-6).

total channel thickness	=	0.25 μ
gate length	=	9.8 μ
built-in voltage	=	-1.0 V.
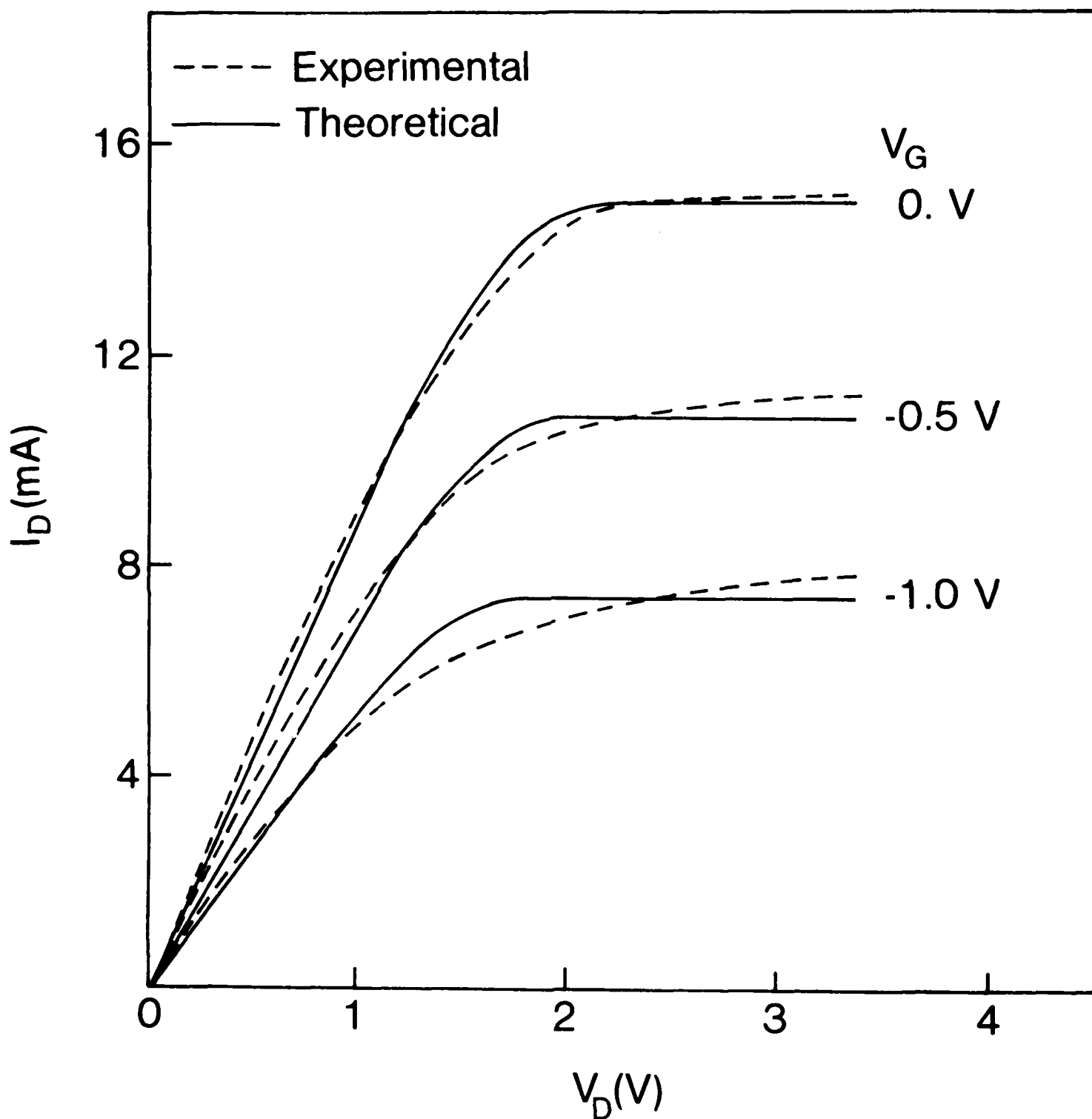
Fig. 6-6 Fit of the I-V data with our model. Solid lines
and dashed lines represent experimental and fitted
theoretical data, respectively. The fitting para-
meters are given in the text.

48

With these parameter values we obtain a very good fit. The LZ model[53] gives a fit five times worse than our model. Considering the uncertainties in the V-E curve and that there is no unphysical parameter in the model, we may say that the parameters obtained and the fit are quite good.

The main reason that the fit gets worse at high gate and drain voltages (V_G and V_D) is that for high V_G and V_D there is some conduction through the substrate and consequently the current (I_D), instead of reaching a saturation, has a small slope. This factor is not incorporated in the model.

6.4 Conclusion

In conclusion, we have shown that for FET's composed of semiconductors like GaAs and InP, the theoretical I-V characteristics can be in error by a large amount if one uses the LZ model, even though the velocity (Eq. 6-1) is correct at very small and very high fields. This error arises because the Trofimenkoff relationship differs from the realistic v-E characteristic for the materials under consideration in the intermediate field region. Using a realistic v-E relationship we have developed a model which gives a good fit with measured I-V data. We hope that this model can be modified and used in analyzing the I-V data of HEMT devices which are under study in the current program.

7.0 QUANTUM WELLS AND SUPERLATTICES

7.1 Introduction

In recent years an intense worldwide effort has been devoted to
the studies of the properties of a new class of man-made materials, called
superlattices. Semiconductor superlattices are formed by growing alternate
layers of two different lattice matched (or slightly mismatched) semicon-
ductors. The most studied system is that of GaAs and $Ga_{1-x}Al_xAs$. Growth
techniques such as Molecular Beam Epitaxy (MBE) or Metal Organic Chemical
Vapor Deposition (MOCVD) make it possible to precisely control concentra-
tion of the components (e.g., of Aℓ in GaAℓAs) and to produce sharp
interfaces. These systems have important practical implications. Owing
to the difference in the band gaps of GaAs and GaAℓAs, carriers (electrons)
from the intentionally doped GaAℓAs region tunnel to the lower energy GaAs
region. Thus, the carriers are geometrically separated from the impurity
ions and thereby the transverse mobility increases tremendously. Exploit-
ing this high mobility and spatial quantization, a number of novel devices
have been made, including high electron mobility transistors (HEMT) and
lasers.

If the GaAs layers are separated by thick layers of GaAℓAs
($>200 A^o$), the carriers in one well region (GaAs) do not feel the presence
of other GaAs regions. Then each GaAℓAs-GaAs - GaAℓAs period can be
thought of as an isolated entity, called a quantum well. Due to the
quasi-two-dimensional nature of the carriers in such quantum wells, the
carriers exhibit various interesting properties which are of fundamental
nature. Thus, studies related to quantum wells and superlattices are
important not only from a practical point of view, but also from a point
of view of basic physics.

50

As in bulk semiconductors, understanding the properties and per-formances of devices made of superlattices depends crucially on the knowl-edge of energy levels, effect of external perturbations on these levels, quality of the interfaces, etc. In the following sections we briefly describe some of the contributions we have made in this area.

7.2 Hydrogenic Impurity Ground State in GaAs-GaAℓAs Multiple-Quantum-Well Structures

The following abstract is reprinted from Ref. 57:

We report the results of a variational calculation for the hydro-genic-impurity ground state in a multiple-quantum-well structure consisting of alternating slabs of GaAs and $Ga_{1-x}Aℓ_xAs$. Calculations have been carried out with the assumption that the impurity envelope wave function spreading beyond the next-nearest-neighbor GaAs wells is negligible. Impurity envelope wave functions have been plotted for some typical GaAs well and $Ga_{1-x}Aℓ_xAs$ barrier thicknesses to find the extent of wave-function spreading. The binding energy is found to vary substantially as a function of the barrier thickness. Calculations are performed for the variations of the binding energy as a function of the well thickness and also as a function of the barrier thickness. The main peak in the impurity binding energy in superlattices with equal well and barrier thickness is shifted towards a thickness larger than that in single-well systems. A secondary peak appears at a very small thickness, which arises because the model includes only three wells. The results of the present calculation in various limiting cases agree with previous results.

The introduction from the same paper is also reprinted.

The recent advances in crystal-growth techniques such as molecular-beam epitaxy and metal-organic chemical-vapor deposition (MOCVD) have made possible the growth of systems consisting of alternate layers of two

51

different lattice-matched semiconductors with very precisely controlled thicknesses and sharp interfaces. Such one-dimensional periodic structures are generally referred to as superlattices. Numerous studies have been devoted to various aspects of the electronic states associated with such systems[58]. Among the superlattices grown, so far, the GaAs-$Ga_{1-x}Al_xAs$ system is the simplest and the most extensively studied. The band gap of $Ga_{1-x}Al_xAs$ increases with the concentration of x of aluminum. Thus there exists a discontinuity of the band edges at the GaAs-$Ga_{1-x}Al_xAs$ interfaces. The conduction-band-edge discontinuity is about 85% of ΔE_g; the band-gap difference between bulk $Ga_{1-x}Al_xAs$ and GaAs. The valence-band-edge discontinuity is about 15% of ΔE_g. As a result, the electrons and holes in a GaAs layer find themselves in approximately rectangular potential wells for sharp interfaces.

Studies of the shallow impurity states in such quantum wells have recently begun with the work of Bastard[59]. He calculated the ground-state binding energy of a hydrogenic shallow impurity in the GaAs quantum well. In that calculation the potential barrier height in the $Ga_{1-x}Al_xAs$ regions was taken to be infinite. He finds that the binding energy increases as the well size (i.e., the GaAs layer thickness) is reduced. Mailhiot, Chang, and McGill[58] (MCM) have done an extensive calculation for the binding energies, wave functions, and their variations with well thickness, impurity position, etc., for realistic finite potential-barrier height, contrary to Bastard's infinite barrier height. They also include the effects due to different effective electronic masses and dielectric constants in GaAs and $Ga_{1-x}Al_xAs$ layers. They have found that the binding energy goes through a maximum as the well size is reduced instead of continuously increasing as is found in the

infinite-barrier calculation. Greene and Bajaj[60] (GB) have also performed a similar calculation for impurities at the center of a quantum well. Both of the groups, MCM and GB, have calculated some excited-state binding energies.

In all of the previous calculations it has been assumed that the $Ga_{1-x}Al_xAs$ layers are thick enough to confine the wave functions so that they do not spill over to the adjacent GaAs quantum wells. Calculations were performed with this assumption for an impurity in a quantum well with two semi-infinite $Ga_{1-x}Al_xAs$ barriers on each side of the well. Super-lattices are made with layer thickness ranging from a few monolayers to about 400 Å. Most attention has been focused on systems with aluminum concentration x of $Ga_{1-x}Al_xAs$ less than 0.45. In this concentration range the band gap is direct at the Γ point[61]. The spreading of the impurity envelope wave functions depends on the potential barrier height as well as the barrier thickness. In general wave functions spread more to the adjacent wells if the barrier height or the thickness is reduced. Thus the previous calculations with single-well approximation are not adequate for thin superlattices, or even for moderately thick superlattices but with small aluminum concentrations. This is evident from the wave-function plot of MCM[58]. In this situation we feel that it is desirable to perform a calculation which should be valid for thin or small barrier-height super-lattices. The present paper, to our knowledge, is the first report of such a calculation. In this calculation we consider for simplicity the impurity to be at the center of a well. Assuming that the spread of the wave functions to the next-nearest-neighbor wells of the one containing the impurity, the calculation has been performed with only one well on each side of the well under consideration.

One of the main features of this calculation is presented in Figure 7-1. The reader is referred to the original Reference 57 for details.

7.3 Effect of Nonparabolicity on the Energy Levels of Hydrogenic Donors and Excitons

The following abstract is reprinted from Reference 62:

Binding energies of the ground state and of a few low-lying excited states of a hydrogenic donor in a quantum-well structure consisting of a single layer of GaAs sandwiched between two semi-infinite layers of $Ga_{1-x}Al_xAs$ are calculated, including the effect of nonparabolicity of the conduction band and following a variational approach. The effect of nonparabolicity of the conduction band is included by using an expression for the energy-dependent effective mass based on the $\bar{k}-\bar{p}$ approximation. The variations of the binding energies of these states as a function of the size of the GaAs quantum well for different values of the potential barrier (or equivalently for different values of Al concentration x) are calculated. These results are compared with those obtained with the use of a parabolic conduction band.

The following abstract is reprinted from Reference 63:

Binding energies of the ground states of Wannier excitons in a quantum well structure consisting of a single layer of GaAs sandwiched between two semi-infinite layers of $Ga_{1-x}Al_xAs$ are calculated including the effects of non-parabolicity of the conduction band, following a variational approach. Due to reduction in symmetry along the axis of growth of these structures and the presence of energy band discontinuities at the interfaces, the degeneracy of the valence band of GaAs is removed, leading to the formation of two types of excitons, namely, the heavy hole exciton and the light hole exciton. The effect of
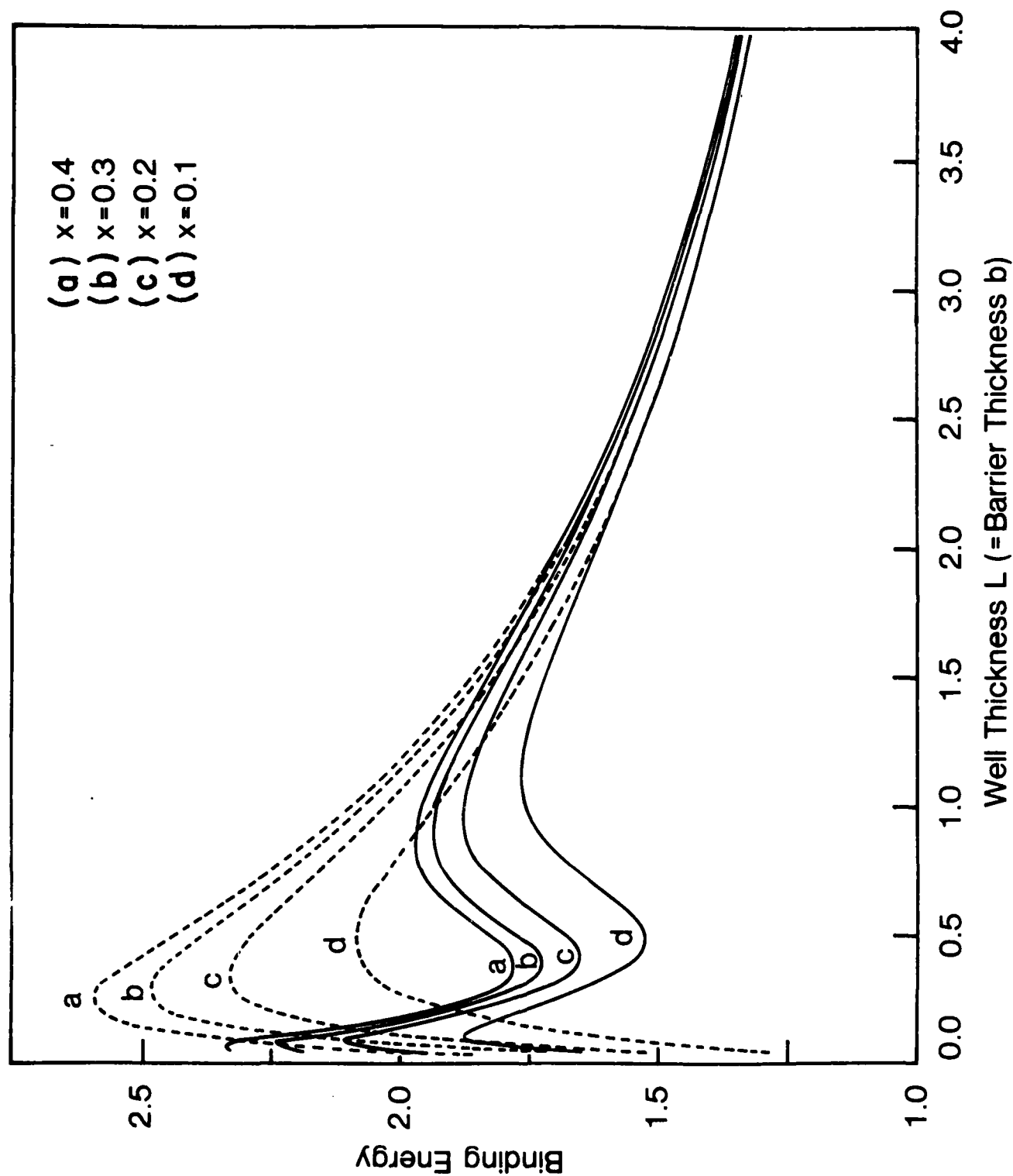
Fig. 7-1 Binding energy for the hydrogenic-impurity ground state as a function of the GaAs layer thickness when the GaAs and $Ga_{1-x}Al_xAs$ layer thicknesses are equal for alloy compositions $x = 0.1$, 0.2, 0.3, and 0.4 of $Ga_{1-x}Al_xAs$.

55

non-parabolicity of the conduction band is included by using an expression for the energy dependent effective mass based on $\vec{k} \cdot \vec{p}$ approximation. The variations of the binding energies of these two excitons as a function of the size of the GaAs quantum well for various values of the heights of the potential barrier are calculated. These results are compared with those obtained using a parabolic conduction band. It is found that the inclusion of the non-parabolicity effect leads to more binding for all values of the quantum well size.

7.4 Effect of Interface Quality on Photoluminescence Lineshape

The following abstract is reprinted from Reference 64:

We have developed a simple theory to understand the role of interfacial quality in the lineshape of photoluminescence spectra in quantum wells. The interface is described in terms of microscopic fluctuations δ_1 and δ_2 where δ_1 is the local fluctuation in the well width and δ_2 is the lateral correlated extent of the fluctuation. We make use of Lifshitz theory of disordered alloys to determine the probability of distribution of fluctuations in the well size over the extent of the optical probe, i.e., the exciton. The lineshape is then calculated from this probability distribution. Both δ_1 and δ_2 are found to be important in controlling the linewidths in quantum wells. The use of this quantitative theory to characterize the microscopic nature of interfaces is discussed.

8.0 SPARK SOURCE MASS SPECTROMETRY

8.1 Background

Spark source mass spectrometry has been utilized for over two decades for the comprehensive elemental characterization of inorganic solid materials, particularly with regard to trace and ultra-trace impurities. The technique features absolute qualitative identification of elemental components, with rapid, simultaneous detection of most elements to 0.1 parts per million, atomic, or lower. The role of the SSMS (MS-702, AEI-CED, Ltd., Manchester, England) facility located at Wright State University has been to assist AFWAL/AADR in the analysis and evaluation of gallium arsenide research materials. Since the type and concentration of many elemental impurities – both doped and residual – are known to drastically affect the electrical properties of GaAs, the basic function of the SSMS effort has been to provide routine, reliable determinations of low-level impurities in GaAs samples. During the past three years, approximately 200 GaAs samples, including thick epitaxial layers, doped samples, and substrate materials, have been analyzed.

8.2 Analytical Program

The SSMS technique has been employed for three primary applications:

1) Routine analysis of high-purity GaAs for residual elemental impurities.

2) The continuation of calibration studies to quantify measurements of elements of interest such as Fe, Mn, Cr, S, Si and B.

3) The development of methodology for determination of trace levels of oxygen and carbon.

In pursuing the first goal, the spark source mass spectrometric technique has been shown to be effective in the rapid determination of a wide range of elemental impurities. As is shown in Table 8-1, detectabilities are frequently less than <0.1 parts per million, atomic (ppma). During the three-year investigation, many GaAs samples were found to contain residual impurities – particularly Fe and Si – which (as revealed by Hall-effect tests) adversely affected the resistivity properties.

In conjunction with the second goal, GaAs wafers were implanted using $^{32}S^{+}$. Additionally, some GaAs samples were implanted using $^{16}O^{+}$. The results obtained from SSMS analyses are shown in Table 8-2. This data shows the SSMS method to be effective in tracking implanted doses and, in the case of $^{16}O^{+}$ a calibration factor ("True" value/Observed value) of 2 - 3.

The third goal sought during the program has involved the utilization of a cryogenic pumping system[65] developed for the MS-702 at Wright State University. A machine modification involved the installation of a turbomolecular vacuum pump (Alcatel Vacuum Products, TMP 140) for the ion source chamber. The purpose was to achieve "cleaner" pumping (reduced hydrocarbon background) than was provided by the standard oil diffusion pump, thereby allowing lower limits of detection for carbon. The addition of turbo pumping along with the liquid helium cryopumping of the ion source region has yielded detectabilities of 0.02 ppma for oxygen and 0.02 - 0.03 ppma for carbon. Along with the ion-implantation experiments described above, GaAs samples (and one Si sample) doped with oxygen or carbon have been analyzed and these efforts are summarized in Table 8-3.

TABLE 8-1. SPARK SOURCE MASS SPECTROSCOPIC DATA IN GaAs

Units: Parts per million atomic (ppma)

S A M P L E   D E S I G N A T I O N

Element	65-2	65-5	65-6	65-7	NRL 16L2-7	NRL 16L29	KAIST 30-3	KAIST Not Annealed	
Be	<0.02	<0.02	<0.01	<0.01	<0.02	<0.02	<0.02	<0.02	
B	0.2	0.1	0.1	0.1	10	10	<0.02	<0.02	
C									
O									
Mg	<0.03	<0.1	<0.03	<0.03	<0.1	<0.1	<0.03	<0.03	
Al	<0.02	<0.02	<0.02	<0.02	<0.03	<0.03	<0.03	<0.03	
Si	0.2	0.2	≤0.1	≤0.1	<0.1	<0.1	<0.1	<0.1	
S	<0.1	<0.1	<0.05	<0.1	<0.1	<0.1	<0.03	<0.03	
Cr	<0.02	<0.02	<0.02	<0.1	0.5	1	<0.02	<0.02	
Mn	<0.02	<0.02	<0.01	<0.01	<0.02	<0.02	<0.02	<0.02	
Fe	0.1	<0.02	<0.02	0.1	<0.03	0.3	<0.02	<0.02	
Co	<0.02	<0.02	<0.01	<0.01	<0.02	<0.02	<0.02	<0.02	
Ni	<0.03	≤0.03	<0.02	<0.02	<0.03	<0.03	<0.03	<0.03	
Cu	<0.03	<0.03	<0.02	<0.02	<0.05	<0.05	<0.05	<0.05	
Zn	<0.06	<0.06	<0.06	<0.06	<0.06	<0.06	<0.06	<0.06	
Ge	<0.2	<0.2	<0.2	<0.2	<0.3	<0.3	<0.3	<0.3	
Se	<0.2	<0.2	<0.2	<0.2	<0.2	<0.2	<0.2	<0.2	
Ag	<0.04	<0.04	<0.02	<0.02	<0.04	<0.04	<0.04	<0.04	
Cd	<0.1	<0.1	<0.04	<0.04	<0.1	<0.1	<0.1	<0.1	
Sn	<0.06	<0.06	<0.03	<0.03	<0.06	<0.06	<0.06	<0.06	
Te	<0.06	<0.06	<0.03	<0.03	<0.06	<0.1	<0.04	<0.04	
Au	<0.02	<0.03	<0.03	<0.02	<0.02	<0.02	<0.03	<0.03	
Hg	<0.1	<0.1	<0.03	<0.03	<0.1	<0.1	<0.1	<0.1	

NOTES: SAMPLES WERE ANLYZED AT ROOM TEMPERATURE.
NRL SAMPLES WERE CR-DOPED.   59

TABLE 8-2. SPARK SOURCE MASS SPECTROGRAPHIC ANALYSIS OF

ION-IMPLANTED GaAs (ppma)

DOSE $\left(\dfrac{300 \text{ Kv } ^{32}S^+}{\text{ions/cm}^2}\right)$	Effective cone (ppma) (Average Sample Thickness)	Observed SSMS Value
1.94×10^{14}	0.1	0.05
5.5×10^{14}	0.3	0.2
1.67×10^{15}	1	1
$\left(\dfrac{300 \text{ KV } ^{16}O^+}{\text{ions/cm}^2}\right)$ *		
1.94×10^{14}	0.1	0.2
5.5×10^{14}	0.3	0.2
1.67×10^{15}	1	0.5
5×10^{15}	3	1

* Samples baked in ion chamber and cryopumped during analysis using

liquid helium.

60

TABLE 8-3.   SSMS ANALYSIS OF GaAs AND Si.   (ppma)

Element	Sample Number	SSMS Value	Accepted Value (If Available)	Value by Other Analyses
C	G694T	3	---------	3 (a)
C	G694E	1	---------	1 (a)
O	A439/8	0.2 (c)	0.25	0.2 – 0.25 (b)
O	Si (d)	2	5	

(a)   Secondary Ion Mass Analysis by C. A. Evans, Associates.
      Samples were C-doped.

(b)   Values by Charged Particle Activ. and SSMS, J. B. Clegg,
      Philips Research Labs, Surrey, U. K., O-doped.

(c)   Repeated in three runs.

(d)   Silicon Sample.

8.3 Summary

Throughout the program, the application of spark source mass spectrometry has been shown to be generally successful in surveying GaAs and other semiconductors for trace impurity content. However, the need for continued calibration efforts using suitably doped samples is clear. During the program, several GaAs, InP, and GaP materials that had been heavily doped with elements such as Fe, Mn, Cr, Si, Zn, Te, Sn, and Ge were analyzed by SSMS and the acquired values used in conjunction with photoluminescence measurements. However, insufficient sample quantity prevented analysis by complimentary analytical techniques. The results in Table 8-3 indicate reasonably good SSMS accuracy for O and C determination when suitable samples are available, and liquid helium cooling and turbomolecular pumping are used. Subsequent SSMS analyses of GaAs samples thought to contain O (as shown by photoluminescence spectra) did not reveal significant O levels. This could be due to greater sensitivity by photoluminescence, in observing O peaks, than SSMS.

9.0 NEW PAIRING STATE, CHARGE DENSITY WAVE, SPIN DENSITY WAVE, PAIRING OF HOLES, AND SUPERCONDUCTIVITY

The following summary is from an invited talk given by S. B. Nam at the 9th International Conference on High Pressure, in 1983:

We have suggested that the pairing of holes[66], or finite momentum pairing(q), or charge density wave (CDW) orders might be responsible for the unusual metastable phenomena observed in pressure quenched CdS[67,68,69]. Furthermore, it is shown that the pair binding energy in one dimension[70] and two dimensions[71], has an extra maximum at the pair momentum, $q_2 = k_F + K_F$, additional to the usual one at $q = 0$, where $K_F = (K_F + 2m\omega_c)^{\frac{1}{2}}$ and ω_c is the usual cut-off energy ($\hbar = 1 = c$). These findings encourage us to believe that there is a possibility of having the finite momentum pairing order. This is what we have found.

The coexistence of CDW and superconductivity has been examined by several people, in one dimension[72], and in A15 compound such as V_3Si[73], and others. Recently the observed Raman lines[74] in $2H-NbSe_2$, can be understood by the CDW induced modes via coupling between the CDW and the superconducting gap excitation, and in a quite different view, also by a collective mode based on the gauge invariant theory[75]. The SO(6) has been identified as a dynamical group of a mean field Hamiltonian of the CDW superconductor[76].

On the other hand, Machida, et al.[77] have suggested the finite momentum pairing in antiferromagnetic superconductors. However, Nass, et al.[78] have pointed out that the calculation of Machida, et al. was in error, and have argued that within their numerical calculation, finite momentum pairing is possible in neither antiferromagnetic[78], nor CDW superconductor[79].

63

But, both groups of Machida, et al. and Nass, et al. have treated the order parameter as real variables. We believe that, physically, the order parameters should be treated as complex variables when both zero and finite momentum pairing orders are present, since the latter is equivalent to having a local current, even though the total current is zero, with the q and -q pairings.

In fact, we have found that the lowest free energy state is indeed the one in which the phases of order parameters have special values. This is the most striking result, in our view. The state with real order parameters turns out not to be the lowest free energy state, when the q order is present with the other orders, such as the BCS, or both CDW and BCS orders.

We have shown that when the q order is present with the other orders, the phases of order parameters play crucial roles for determining the ground state, and that the excitation energy and effective energy gap are oscillating.

10.0   ORIGIN OF THE X-CENTERS IN SILICON AND GERMANIUM; SOLITON

For the last several years, there have been reported the unknown X-centers in doped silicon[80-83], and doped germanium[84-85]. Several attempts with models of complexes have been made to understand the X-centers with qualitative success[80, 82]. It has been an important problem to understand the X-centers since the above materials have been used for sensitive IR detectors. The materials with the X-centers cannot be used for such detectors, since an unwanted noise is produced via the X-centers.

Recently, Ohmer and Lang[86] have been able to obtain a good agreement between the calculated and observed X-center energies for the majority of data, using an emperical relation:

$$E_x - E_x^G = \tfrac{1}{2}(E_A + E_B) - \tfrac{1}{2}(E_A^G + E_B^G) \qquad , \qquad (10\text{-}1)$$

where E_x, E_A, and E_B are the energies of the X-center, and of two appropriate acceptors A and B, respectively. The superscript G stands for the respective ground states.

We present here a physical picture leading to the above emperical relation by demonstrating a possibility of having the distortion-induced soliton. By no means is our description a complete answer. Perhaps, it will give a direction by which the understanding of the X-centers will be enriched.

Our physical scenario goes as follows: When a distortion is introduced in the system via doping, or irradiation, or other means, the probability of transferring a hole from the acceptors A to B, or vice versa, will be increased. Of course, the same argument will, equally well, apply to the case of electrons from two appropriate donors. If the transfer-integral energy exceeds the energy difference between the levels of two

acceptors, $\frac{1}{2}(E_A - E_B)$, then a new order ground state sets in, and a soliton state is predicted to occur with the energy of $\frac{1}{2}(E_A + E_B)$. This yields the empirical relation of Eq. 10-1.

The two appropriate states, of course, are the same symmetry states from acceptors A and B, since other combinations will have negligibly small or zero overlapping integrals of wave functions. We thus discuss the two same symmetry states, from two appropriate acceptors, for our purposes.

The Hamiltonian of the system can be written with $\phi^+ = (C_A^+, C_B^+)$ as

$$H = \Sigma \ \phi^+ \ \sigma_3 \ \varepsilon \ \phi + D^2 + H_{hD} \tag{10-2}$$

$$H_{hD} = - \ \Sigma \ g^{\frac{1}{2}} \ D \ C_A^+ \ C_B + c.c.$$

where C_i^+ and C_i (i = A, B) are the usual creation and annihilation operators for holes, and σ_i (i = 1,2,3) are the 2x2 Pauli matrices. The second term is the distortion energy and H_{hD} is the transfer coupling energy between the distortion field D and holes, with the transfer integral energy g. The ε is $\frac{1}{2}(E_A - E_B)$, and the zero energy is chosen at $\frac{1}{2}(E_A + E_B)$, with the positive energy axis opposite to that of the electron. The summation should be understood in the usual manner over the up and down states of holes, for simplicity. The distortion field can be from the lattice distortion, or the distortion of acceptor positions from their equilibrium positions.

Using the usual commutation of C_i with H, one gets the eigenvalue equation,

$$(\sigma_3 \ \varepsilon + \sigma_1 \ \Delta) \ \phi = E \ \phi \tag{10-3}$$

with $\Delta = <- g^{\frac{1}{2}} D >$, where $< >$ denotes the grand canonical ensemble average.

We easily get the eigenvalues $\pm E$ and the spinor solution $\phi^+ = (u, v)$ as

$$E = (\varepsilon^2 + \Lambda^2)^{\frac{1}{2}} \tag{10-4}$$

$$u^2 = 1 - v^2 = (1 + \varepsilon/E)/2$$

with sign (v) = sign (Δ). The Hamiltonian Eq. 10-2 can be rewritten, in terms of new Fermion operators $(a_1^+, a_2^+) = (C_A^+, C_B^+)(u + i\sigma_2 v)$, and $n_i = a_i^+ a_i$ $(i = 1,2)$ as

$$H = \Sigma E(n_1 - n_2) + D^2 \tag{10-5}$$

In the ground state, $|\Pi a_2^+ >$, we get $n_1 = 0$, and $n_2 = 1$, so that the new up and down states are occupied. The ground state energy $W(D)$ is given as

$$W(D) - W(0) = 2(\varepsilon - E) + D^2 \tag{10-6}$$

This has a maximum at $D = 0$, and a minimum value

$$W(\pm D_m) - W(0) = - E(1 - \varepsilon/E)^2 \tag{10-7}$$

at $D = \pm D_m$, as shown in Figure 10-1, with the condition

$$\Delta^2 = g^2 - \varepsilon^2 = g D_m^2. \tag{10-8}$$

The above condition is essential for our discussion. In order to have an order parameter Δ, the ε should be less than g. When it is such a new order ground state sets in, so that the distorted state $(D \neq 0)$ becomes the lowest energy state, in analogy to a charge density wave, or the theory of superconductivity. Note that there are double minima

67
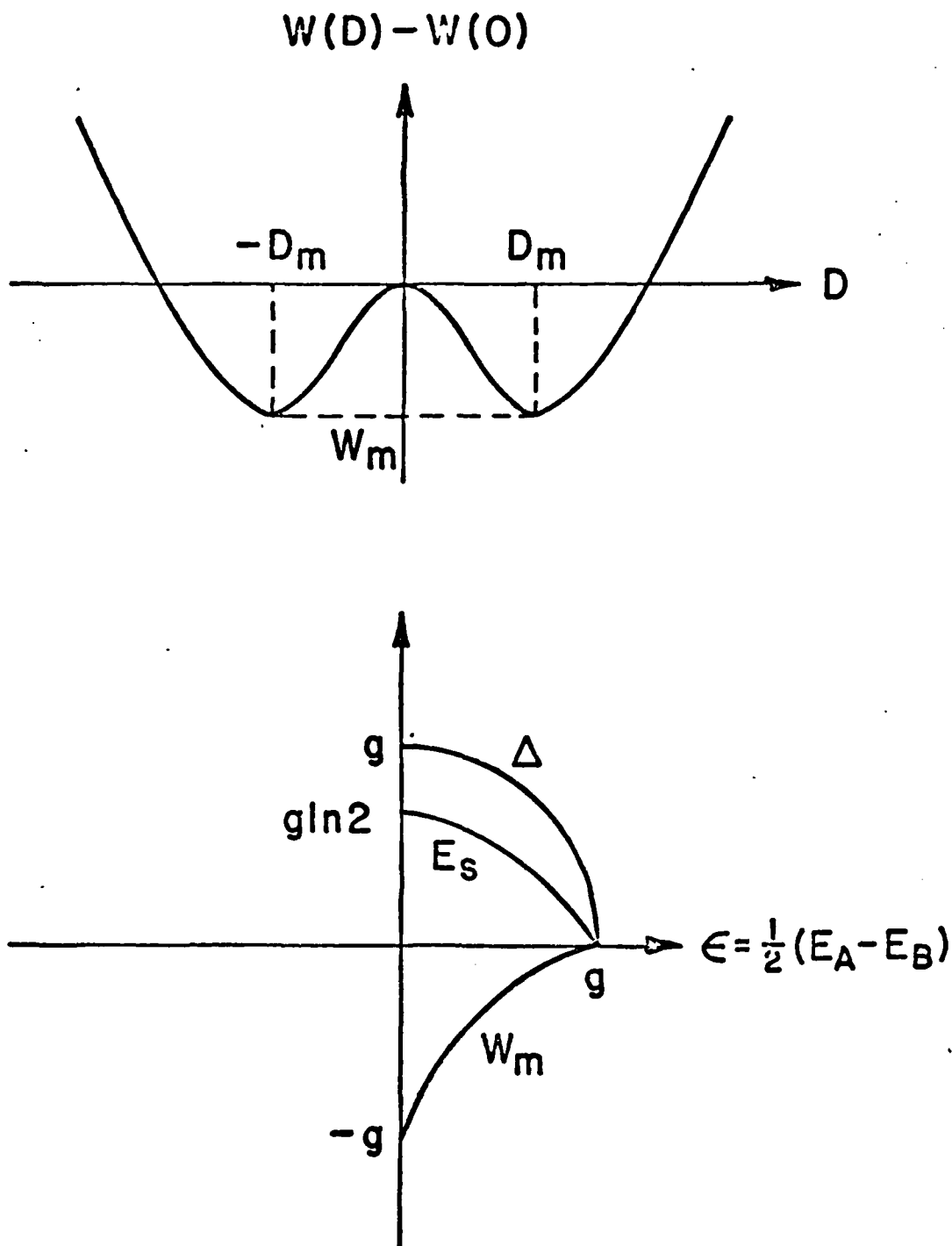
Fig. 10-1 The ground state energy as a function of D is in
the upper graph. The order parameter Δ, soliton
formation energy E_s, and the minimum ground state
energy W_m as functions of energy difference ε are
shown in the lower graph.

68

$D = + D_m$. If we consider the distortion of distance between two appropriate acceptors for the distortion field, then there are two separation distances with the same energy of the system. This double degeneracy leads to a soliton state. In other words, one configuration state is dominant in one region, and another state in a different region, and so on. The topological excitation-soliton comes in.

We now show that a soliton solution exists at $\frac{1}{2}(E_A + E_B)$. For this, we consider the Hamiltonian Eq. 10-2 in real space. The potential energy contributions from both acceptors and ion energies can be lumped into the effective interaction and effective distortion energies.

We easily get the eigenvalue equation in real space, corresponding to Eq. 10-3:

$$\{\sigma_3 \, \varepsilon + \sigma_1 \, \Lambda(R,r)\} \, \phi_n = E_n \, \phi_n \tag{10-9}$$

with the spinor $\phi^+ = \{ U*(R,r), V*(R,r)\}$ and the self-consistent condition,

$$\Lambda(R,r) = \Sigma \, (-g)U(R,r)V*(R,r). \tag{10-10}$$

The energy difference factor ε may be written as $\varepsilon = (-h^2/2m_h)\partial_R\partial_r$, where m_h is the effective hole mass, $R = (r_A + r_B)/2$, and $r = r_A - r_B$, with respective hole coordinates r_A and r_B . For simplicity, we consider a quasi-one dimension in the direction of separation of two appropriate acceptors. Taking the Fourier transformation via $\exp(ik_i x_i)$, where $x_i = r$, or R, and with the characteristic wave vector k_i , we get $\varepsilon = (\hbar k_i/2m_h) (- \hbar\partial_j)$. Equation 10-9, with the above ε, becomes identical to the spinless Dirac equation discussed by Jackiw and Rebbi[87] who have found a soliton solution for $E_n = 0$, with $\Lambda(x_i) = \Lambda_o \tanh(x_i/\xi)$

69

and a soliton to have $\frac{1}{2}$ Fermion number, equivalently $\frac{1}{2}e$ charge. The length parameter ξ can be considered as a variational parameter. For solitons in polyacetylene[88, 89], the lowest soliton formation energy $E_s = (2/\pi)\,\Lambda_\infty$ is found when $\xi = \hbar\, v_F/\Lambda_\infty$. We now estimate the soliton formation energy,

$$E_s(\varepsilon) = W(\Lambda \tanh x_i/\xi) - W(\Lambda) \tag{10-11}$$

with $\Lambda = (g^2 - \varepsilon^2)^{\frac{1}{2}}$ from Eq. 10-8. Since $\Delta(\varepsilon) < \Delta(0)$, we expect $E_s(\varepsilon)$ to be less than $E_s(0)$. By taking a mean value of $E_s(0)$ over the character-istic length, we easily get $E_s(0) = g\,\ln2$, less than g.

We thus can have a soliton solution at $\frac{1}{2}(E_A + E_B)$, with $g > \varepsilon$. The emperical relation of Eq. 10-1 is justified in our physical picture of solitons.

We remark that the interaction and distortion energies in Eq. 10-2 can be derived microscopically in the spirit of Anderson[90]. When a distortion d is introduced in the system, the coupling and distortion energies can be written by $2g_0^{\frac{1}{2}}d(n_A + n_B) + d^2$, with $n_i = c_i^+ c_i$ (i = A, B). Minimiz-ing it with respect to d, and together with the Coulomb energy $U_c n_A n_B$, we get $-g_0(n_A + n_B) - g\,n_A n_B$, with the effective coupling $g = 2g_0 - U_c$. The first term can be lumped into E_A and E_B without changing ε in Eq. 10-2. The rest may be written after factorizing as

$$-g n_A n_B \rightarrow \Delta\, c_A^+ c_B + \Delta^* c_B^+ c_A + |\Delta|^2/g \tag{10-12}$$

with $\Delta = \langle \sum (-g)\, c_B^+ c_A \rangle$. The above is identical to the one used in Eq. 10-2. In particular, for $2g_0 > U_c$, the effective interatction between n_A and n_B becomes attractive. This is precisely the origin of superconduc-tivity with the electron phonon interaction $2g_0$ being greater than U_c.

70

Also, it leads to the double charge state of the so-called Anderson U-center.

We can easily extend our argument to the case of diatomic polymer chains without difficulty. In this case, the periodicity generates the usual energy dispersion for the conduction and valence bands and the energy difference ε comes in as a parameter. We will have soliton solutions at $\pm\varepsilon$ (at E_A and E_B), respectively.

Finally, since the excited state, $E^1\Sigma_g$, of the hydrogen molecule H_2, has two minima in the potential energy[91] at two separation distances between two nuclei, it is predicted that a soliton state is possible in the H_2-system as well.

11.0   A COHERENT EXCITATION STATE AND ANISOTROPIC RAMAN

SCATTERING EFFICIENCIES IN n- GaAs

A coherent excitation state has been introduced to understand the anisotropic Raman scattering efficiencies in n-GaAs under the resonance condition[92].

In the Raman scattering (with the K_r-6471Å-laser) by coupled plasmon LO phonon modes in n-GaAs samples with $n = 3.1 \sim 14 \times 10^{17}$ cm^{-3}, the Raman peak due to the L^+- mode is observed in the X(Y, Y + Z) $\overline{X}$ configuration, at 300 K and 77 K, where X = (100), Y = (011), Z = (01$\overline{1}$), and $\overline{X}$ = ($\overline{1}$00). However, the Raman peak due to the L^-- mode is larger in the X(Z, Y + Z)$\overline{X}$ configuration. With the K_r-6764Å-laser, the above anisotropic behavior is observed only at 300 K.

A qualitative understanding of the anisotropic Raman efficiencies may be described at follows: The optical scattering efficiency of Raman processes in a semiconductor, such as n-GaAs, is known to depend upon the thickness, L, of the depletion layer, and the absorption length, ℓ. In particular, the coupling of the plasmon and phonon would occur only in the region of ℓ-L. The size of this optical active region would be sensitive to the dangling band and surface states, since the band-bending behavior depends on them.

On the GaAs (110) surface, the 1 x 1 surface reconstruction has been observed, and the 2 x 2 on the (111) Ga surface, but only the 1 x 1 on the (111) As surface. On the other hand, the 2 x 8 reconstruction has been reported on the GaAs (100) surface of Ga, or As. Thus, the asymmetrical behavior of the optical scattering efficiency is predicted to occur on the (100) surface of GaAs, but not on the (110) and (111) planes.

From a formal point of view[93], the Raman scattering tensor in the back scattering $X(\ ,\ )\overline{X}$ configuration can be written as

$$
\begin{pmatrix} 0 & 0 & 0 \\ 0 & 0 & D \\ 0 & D & 0 \end{pmatrix} + i \begin{pmatrix} D_e & 0 & 0 \\ 0 & D_e & 0 \\ 0 & 0 & D_e \end{pmatrix}
$$

with $D = \partial\alpha/\partial u + \partial\alpha/\partial\in = d\,\exp\,(i0)$

$$D_e = D_\rho + D_F = d_e\,\exp\,(i\phi)\ ,$$

where $\partial\alpha/\partial u$, $\partial\alpha/\alpha \in$, D_ρ , and D_F are due to the deformation potential, electro-optic, charge density fluctuation, and Fröhlich interaction contributions.

The Raman scattering efficiencies in the $X(Y,\ Y + Z)\overline{X}$ and $X(Z,\ Y + Z)\overline{X}$ configurations become proportional to

$$|D \pm iDe|^2 = d^2 + d_e^2 \pm 2dd_e\sin\,(0-\phi)\ .$$

In the non-resonance condition, $d \gg d_e$, we expect no anisotropic behavior in the Raman scattering efficiencies. However, under the resonance condition, the d_e can be of the order of d , and a coherent state comes in; then the anisotropic behavior in the Raman scattering efficiencies is predicted to occur. In particular, the largest anisotropy will occur when $0 - \phi = \Pi/2$.

We believe that the preliminary data[92] can be understood via a coherent state under the resonance condition. It is highly desirable to carry out further study along the above lines.

73

12.0 SUPERLATTICE STRUCTURE AND SUPERCONDUCTIVITY IN HIGH PRESSURE QUENCHED CADMIUM SULFIDE

One of the intriguing aspects of the diamagnetic anomaly observed at 77 K in high pressure quenched cadmium sulfide is the possibility of having high temperature superconductivity[94, 95]. We report here our observation of large diamagnetism in high-pressure-quenched cadmium sulfide at 77 K, indicating possible superconductivity at high temperature, or a new condensed state[96], and our discovery of the two new types of commensurate and incommensurate superlattice structures in cadmium sulfide via the X-ray diffractometer.[97]

12.1 A New Condensed State – Superconductivity

Recently, the evidence for superconductivity at 77 K in high pressure quenched CdS has been reported[94, 95]. The magnetization of pressure quenched CdS samples appears to be like that of a type II super-conductor, and disappears after a few days. It is suggested that this metastable phenomenon may be attributed to the notion of finite momentum pairing, i.e., pairing of holes[98]. We describe here our observation of such large diamagnetism, not inconsistent with superconductivity.

Our method of pressure quenching is quite different from that of Homan et al.[94, 95] whose pressure quenching was carried out at a rate of 10^6 bar/sec, at room temperature. Our pressure quenching was carried out at 77 K by opening the pressure oil valve after the pressure bomb (in the range of 30 ~ 50 Kbar) was immersed in liquid nitrogen; then, the bomb was disassembled. For the pressure transmitting fluids, NaCl and AgCl were used. We are not able to say which quenching method is better. We prefer the pressure quenching at 77 K, since a structural phase transition is known to occur around 80 ~ 150 K in CdS.

The starting materials were pure and doped (Li, Cl, and other elements), CdS grown approximately 15 years ago, and also powder CdS from Alfa Inorganic stock No. 20130.

The measurement of the ac (33 Hz) magnetic susceptibility of the sample was carried out by using pick-up coils and a lock-in amplifier PAR Model 124A. The reference signal was picked from a 20 Ω resistance connected in series with the primary coil. The inductive part of the signal from the secondary coil was chosen to correspond to the real part of the magnetic susceptibility of the sample. All data were taken after the pick-up coils and the samples were immersed in liquid nitrogen. For the calibration of susceptibility, a 7 mg sample of $MnCl_2$ was used.

Some pressure-quenched samples were found to have a diamagnetic susceptibility of $\chi_d = (-\frac{1}{4}\pi)(0.1 \sim 0.2)$, and others to have a paramagnetic susceptibility of $\chi_d \sim 0.07$. The magnetization has disappeared after a day or so for diamagnetized samples, and after a somewhat longer time for paramagnetized ones.

We have examined possible spurious signals due to the following: (a) coil instability, (b) temperature instability, (c) oxygen in liquid nitrogen, (d) liquid oxygen in sample holder, and (e) contamination of magnetic impurities, such as Fe, Co, and other elements. For (a) and (b), the stability was tested before taking a signal from the samples. For (c) and (d), we used fresh liquid nitrogen, and tested the empty sample holder. (e) is irrelevant for the diamagnetic signal, and unlikely to affect any signals, since the magnetization has disappeared after a few days.

Our result is not inconsistent with the reported superconductivity in pressure quenched CdS at 77 K[94, 95]. An X-ray examination of the samples is described in the next section.

12.2 Commensurate and Incommensurate Superlattice Structures

Cadmium sulfide is known to have a wurtzite structure with a = 4.136 A and c = 6.713 A at ambient pressure, zinc blende with a = 5.818 A under pressure, and rocksalt structure with a = 5.464 A under high pressure, above 30 Kbar.

The low-angle X-ray diffraction lines associated with commensurate superlattice structures via an X-ray diffractometer are observed at nd_{hkl}:

Wurtzite	Zinc blende	rocksalt
$2\ d_{110}$	$2\ d_{220}$	$2\ d_{111}$
$3\ d_{110}$	$3\ d_{220}$	$3\ d_{111}$
$2\ d_{101}$	$4\ d_{311}$	
$2\ d_{100}$		
$3\ d_{101}$		

For the rocksalt structure, a line associated with the commensurate index n = 3 has been reported[99]. However, the lines associated with the commensurate indices n = 2 and 3, with hexagonal as well as cubic structures, are observed for the first time, to our knowledge, in cadmium sulfide.

The X-ray diffraction lines associated with an incommensurate superlattice structure, via the X-ray diffractometer, are observed in high pressure (above 30 Kbar) quenched cadmium sulfide (black metallic luster) at

d/Λ	I/I₁	d/Λ	I/I₁
8.890	100	2.614	10
4.439	20	2.592	10
3.100	10	2.386	10
2.884	20	2.212	5
2.679	5	1.977	5

The line at d = 8.890 Å is found to have an intensity stronger than those of the regular strong lines at d = 3.583, 3.557, and 3.16 Å in cadmium sulfide.

We have ruled out, at the present time, the polymorphism and polytypism in cadmium sulfide, since the strong sharp line at d = 8.890 Å cannot be present in those structures. We conjecture that a simple fcc structure with many atoms in the unit cell would be formed in high pressure quenched cadmium sulfide.

It is highly speculated that the superlattice structure would make the effective density of states at band edges increase and also make the number of degenerate intervalleys increase so that high temperature super-conductivity would be realizable[100].

REFERENCES

1. For a recent discussion of these matters, see:

   D.C. Look in Semiconductors and Semimetals, Vol. 19, ed. by R, K. Willardson and A.C. Beer (Academic, New York, 1983) pp. 75-170.

2. D.C. Look, Phys. Rev. B 24, 5852 (1981).

3. B.R. Nag, Electron Transport in Compound Semiconductors (Springer, New York, 1980).

4. D.L. Rode, Phys. Rev. B 2, 1012 (1970).

5. J.R. Meyer and F.J. Bartoli, Solid State Commun. 41, 19 (1982).

6. H.J. Lee and D.C. Look, J. Appl. Phys. 54, 4446 (1983).

7. D.C. Look J.W. Farmer, J. Phys. E.: Scien. Instr. 14, 472 (1981).

8. D.C. Look and P.C. Colter, Phys. Rev. B 28, 1151 (1983).

9. D.C. Look, D.C. Walters, and J.R. Meyer, Solid State Commun. 42, 745 (1982).

10. D.C. Look, S. Chaudhuri, and J.R. Sizelove, Appl. Phys. Lett. 42, 829 (1983).

11. A good discussion of profiling techniques and apparatus may be found in the monograph of H. H. Wieder, Laboratory Notes on Electrical and Galvanomagnetic Measurements (Elsevier, New York, 1979).

12. J.R. Sites and H.H. Wieder, IEEE Trans. Electron Devices, ED-27, 2277 (1980).

13. P.R. Jay and R.H. Wallis, IEEE Electron Device Lett. EDL-2, 265 (1981).

14. D.C. Look, J. Phys. Chem. Solids 36, 1311 (1975).

15. D.C. Look, Phys. Rev. B 25, 2920 (1982).

16. D.C. Look, S. Chaudhuri and L. Eaves, Phys. Rev. Lett. 49, 1728 (1982).

17. See, for example, Semi-Insulating III-V Materials, edited by G. J. Rees (Shiva, Orpington, U. K., 1980).

18. J. Hallais, A. Mircea-Roussel, J.P. Farges, and G. Poiblaud, in Gallium Arsenide and Related Compounds (St. Louis 1976), edited by L. F. Eastman (Institute of Physics, London, 1976), p. 220.

19. R. Zucca, in Ref. 2, p. 228.

20. P.W. Yu and Y.S. Park, J. Appl. Phys. 50, 1097 (1979).

21. P.B. Klein, P.E.R. Nordquist, and P.G. Siebenmann, J. Appl. Phys. 51, 4861 (1980).

22. A. Mircea-Roussel, G. Jacob, and J.P. Hallais, in Semi-Insulating III-V Materials (Nottingham, 1980), edited by G.J. Rees (Shiva, Nantwich, U. K. 1980), p. 133.

23. J.B. Clegg, G.B. Scott, J. Hallais, and A. Mircea-Roussel, J. Appl. Phys. 52, 1110 (1981).

24. T. Itoh and M. Takeuchi, Jpn. J. Appl. Phys. 16, 227 (1976).

25. E.V.K. Rao and N. Duhamel, J. Appl. Phys. 49, 3548 (1978).

26. W.Y. Lum, H.H. Wieder, W.H. Koschel, S.G. Bishop, and B.D. McCombe, Appl. Phys. Lett. 30, 1 (1977).

27. W.Y. Lum and H.H. Wieder, J. Appl. Phys. 49, 6187 (1978).

28. W.Y. Lum and H.H. Wieder, Appl. Phys. Lett. 31, 213 (1977).

29. M. Otsubo, H. Miki, and S. Mitsui, Jpn. J. Appl. Phys. 16, 1957 (1977).

30. D.C. Look, P.W. Yu, J.E. Ehret, Y.K. Yeo, and R. Kwor, in Semi-Insulating III-V Materials, Evian, 1982, ed. by S. Makram-Ebeid and B. Tuck (Shiva, Nantwich, U. K. 1982), p. 372.

31. P.W. Yu, D.E. Holmes and R.T. Chen in GaAs and Related Compounds - 1981, edited by T. Sugano, IOP Conf. Proc. No. 63 (IOP, Bristol and London, 1982) p. 209.

32. P.W. Yu, Solid State Commun. 43, 953 (1982).

33. P.W. Yu, Appl. Phys. Lett. 1984 February issue.

34. J.R. Oliver, R.D. Fairman, R.T. Chen, and P.W. Yu, Elect. Lett 17, 839 (1981).

35. P.W. Yu and D.C. Walters, Appl. Phys. Lett. 41, 863 (1982).

36. P.W. Yu, in Semi-insulating III-V Materials, edited by S. Makram-Ebeid and B. Tuck (Shiva, Nantwich, U. K., 1982) p. 305.

37. D.E. Holmes, R.T. Chen, K.R. Elliot, C.G. Kirkpatrick and P.W. Yu, IEEE MTT-30, 949 (1982).

38. R.J. Wagner, J.J. Krebs, G.N. Stauss and A.M. White, Solid State Comm. 36, 15 (1980).

39. R. Wörner, U. Kaufman, and J. Schneider, Appl. Phys. Lett. 40, 143 (1982).

40. P.W. Yu and D.C. Reynolds, J. Appl. Phys. 53, 1263 (1982).

41. P.W. Yu, W.C. Mitchel, M.G. Mier, S.S. Li, and W.L. Wang, Appl. Phys. Lett. 41, 532 (1982).

42. P.W. Yu, Phys. Rev. B 27, 7779 (1983).

43. P.W. Yu and E. Kuphal, to be published in Solid State Comm.

44. W.M. Theis, K.K. Bajaj, C.W. Litton, and W.G. Spitzer, Appl. Phys. Lett. 41, 70 (1982).

45. W.M. Theis, K.K. Bajaj, C.W. Litton, and W.G. Spitzer, Physica 117B, 116 (1983).

46. See for example, F. Thompson and R.C. Newman, J. Phys. C 5, 1999 (1972), and A.S. Barker, Jr., and A.J. Sievers, Rev. Mod. Phys. 47, No. 2, 1975.

47. R.S. Leigh and R.C. Newman, J. Phys. C: Sol. St. 15, L1045 (1982).

48. P. Kleinert, Phys. Stat. Sol. B 119, K37 (1983).

49. P. Kleinert, Phys. Stat. Sol. B, 117, K91 (1983).

50. W.M. Theis and W.G. Spitzer, J. Appl. Phys., to be published.

51. M.R. Brozel, R.C. Newman, and B. Obzay, J. Phys. C. 12, L785 (1979).

52. W. Shockley, Proc. Inst. Radio Engrs. 40, 1365 (1952).

53. K. Lehovec and R. Zuleeg, Solid St. Electron. 13, 1415 (1970).

54. S. Chaudhuri and D.C. Look, Solid St. Electron. 26, 811 (1983).

55. H. Kroemer, IEEE Trans. Electron. Dev. ED-15, 819 (1968).

56. P.M. Smith, M. Inoue, and J. Frey, Appl. Phys. Lett. 37, 797 (1980).

57. S. Chaudhuri, Phys. Rev. B28, 4480 (1983).

58. C. Mailhiot, Y-C. Chang, and T.C. McGill, Phys. Rev. B26, 4449 (1982); and references therein.

59. G. Bastard, Phys. Rev. B24, 4714 (1981).

60. R.L. Greene and K.K. Bajaj, Solid State Commun. 45, 825 (1983).

61. H.C. Casey and M.B. Panish, Heterostructure Lasers (Academic, N.Y., 1978), Pt. A.

62. S. Chaudhuri and K.K. Bajaj, Phys. Rev. B (in press).

63. S. Chaudhuri, K.K. Bajaj, and R.L. Greene, submitted for publication in Solid State Commun.

64. J. Singh, K.K. Bajaj, and S. Chaudhuri, Appl. Phys. Lett. (in press).

65. D.C. Walters, D.C. Look, and T.O. Tiernan, Anal. Letters 16, A17 (1983).

66. S.B. Nam, Physica 107B, 715 (1981).

67. C.G. Homan, K. Laojndapum, and R.K. MacCrone, Physica 108B, 9
(1981). P.J. Cote, C.G. Homan, W.C. Moffat, S. Block, G.P. Piermarini,
and R.K. MacCrone, Phys. Rev. B28, 5041 (1983).

68. E. Brown, C.G. Homan, and R.K. MacCrone, Phys. Rev. Lett. 45, 478
(1980).

69. S.B. Nam, Y. Chung, and D.C. Reynolds, (unpublished), reported at the
U. S. Army Symposium on High Pressure Phenomena, Rensselaerville
N.Y. (June 16-19, 1981), S.B. Nam, Technical Report-DAAA22-81-M-5322
(U.S. Army).

70. S.B. Nam and D.W. Allender, Preprint: Bull. Am. Phys. Soc. 27, 156
(1982).

71. S.B. Nam, (Unpublished), D. Shankland and S.B. Nam, Bull. Am. Phys.
Soc. 27, 156 (1982).

72. K. Levin, D.L. Mills, and S.L. Cunningham, Phys. Rev. B10, 3821, 3832
(1974).

73. G. Bilbro and W.L. McMillan, Phys. Rev. B14, 1887 (1976).

74. R. Sooryakumar and M.V. Klein, Phys. Rev. Lett. 45, 660 (1980); Phys.
Rev. B23, 3213 (1981);(with R.F. Frindt) ibid. B23, 3222 (1981).

75. B. Littlewood and C.M. Varma, Phys. Rev. Lett. 47, 811 (1981).

76. J.L. Birman and A.I. Soloman, Phys. Rev. Lett. 49, 230 (1982).

77. K. Machida, K. Nokura, and T. Matsubara, Phys. Rev. Lett. 44, 821
(1980); Phys. Rev. B22, 2307 (1980).

78. M.J. Nass, K. Levin, and G.S. Grest, Phys. Rev. Lett. 46, 614 (1981);
Phys. Rev. B25, 4541 (1982).

79. G.S. Grest, K. Levin, and M.J. Nass, Phys. Rev. B25, 4562 (1982).

80. R. Baron, J.P. Baukus, S.D. Allen, T.C. McGill, M.H. Young, H. Kimura,
H.V. Winston, and O.J. Marsh, Appl. Phys. Lett. 34, 257 (1979).

81. R.N. Thomas, T.T. Braggins, H.M. Hobgood, and W.J. Takei, J. Appl.
Phys. 49, 2811 (1978).

82. C.E. Johnes, D. Schaper, W. Scott, and R.J. Hager, J. Appl. Phys. 52,
5148 (1981).

83. J.J. Rome, W.C. Mitchel, G.J. Brown, D.W. Fisher, M.C. Ohmer, and
T.L. Peterson, Appl. Phys. Lett. 41, 254 (1982).

84. E.E. Haller and W.L. Hansen, Solid State Commun. 15, 687 (1974).

85. M.S. Skolnick, L. Eaves, R.A. Stradling, J.C. Portal, and S. Askenazy, Solid State Commun., 15, 1403 (1974).

86. M.C. Ohmer and J.E. Lang, Appl. Phys. Lett. 34, 750 (1979).

87. R. Jackiw and C. Rebbi, Phys. Rev. D13, 3398 (1976).

88. W.P. Su, J.R. Schrieffer, and A.J. Heeger, Phys. Rev. Lett. 42, 1098 (1979); Phys. Rev. B22, 2099 (1980).

89. H. Takayama, Y.R. Lin-Liu, and K. Maki, Phys. Rev. B21, 2388 (1980).

90. P W. Anderson, Phys. Rev. Lett. 34, 953 (1975).

91. J. Gerhauser and H.S. Taylor, J. Chem. Phys. 42, 3621 (1965).

92. C.Y. Chen, Y.S. Park, and S.B. Nam. Bull. Am. Phys. Soc. 27, 336 (1982).

93. S.B. Nam, (to be published).

94. E. Brown, C.G. Homan, and R.K. MacCrone, Phys. Rev. Lett. 45, 478 (1980).

95. P.J. Cote, C.G. Homan, W.C. Moffatt, S. Block, G.P. Piermarini, and R.K. MacCrone, Phys. Rev. B28, 5041 (1983).

96. S.B. Nam, Y. Chung, and D.C. Reynolds, Proc. 9th Int. Conf. High Pressure, 1983.

97. S.B. Nam, T. Mah, R. Crane, Y. Chung, and D.C. Reynolds, Proc. 9th Int. Conf. High Pressure, 1983.

98. S.B. Nam, Physica 107B, 715 (1981).

99. J.A. Corll, J. Appl. Phys. 35, 3032 (1964).

100. S.B. Nam, Proc. 9th Int. Conf. High Pressure, 1983.

PUBLICATIONS

1. D.C. Look, "The Statistics of Multi-Charge Centers in Semiconductors:
    Applications," Phys. Rev. $\underline{B24}$, 5852 (1981).

2. J.R. Oliver, R.D. Fairman, R.T. Chen and P.W. Yu, "Undoped Semi-insu-
    lating LEC GaAs," Elect. Lett. $\underline{17}$, 839 (1981).

3. D.E. Holmes, R.G. Wilson and P.W. Yu, "Redistribution of Fe in InP
    during liquid phase epitaxy," J. Appl. Phys. $\underline{52}$, 3396 (1981).

4. D.C. Look, "Magneto-Hall and Magnetoresistance Coefficients in Semi-
    conductors with Mixed Conductivity," Phys. Rev. $\underline{B25}$, 2920 (1982).

5. D.C. Look, D.C. Walters, and J.R. Meyer, "A Dominant Electrical
    Defect in GaAs," Solid State Commun. $\underline{42}$, 745 (1982).

6. D.C. Look, P.W. Yu, J.E. Ehret, Y.K. Yeo, and R. Kwor, "A Detailed
    SI GaAs Substrate Study: Conversion and MESFET Properties," in
    Semi-Insulating III-V Materials, Evian, 1982, ed. by S. Makram-Ebeid
    and B. Tuck [Shiva, Nantwich (U.K.), 1982] p. 372.

7. D.C. Look, S. Chaudhuri, and L. Eaves, "Positive Identification of the
    $Cr^{4+} \to Cr^{3+}$ Thermal Activation Energy in GaAs," Phys. Rev. Lett. $\underline{49}$,
    1728 (1982).

8. P.C. Colter, C.W. Litton, D.C. Reynolds, D.C. Look, P.W. Yu, S.S. Li,
    and W.L. Wang, "Novel $Ga/AsCl_3/H_2$ reactor for controlling stoichiome-
    try in the growth of vapor phase epitaxy (VPE) GaAs," Proc. of SPIE
    $\underline{323}$, 28 (1982).

9. P.W. Yu and D.C. Reynolds, "Photoluminescence identification of ~
    77 meV deep acceptor in GaAs," J. Appl. Phys. $\underline{53}$, 1263 (1982).

10. P.W. Yu, D.E. Holmes and R.T. Chen, "Photoluminescence Study in LEC
    GaAs," Int. Conf. GaAs and Related Compounds, Japan, 1981, Inst. Phys.
    Conf. Ser. $\underline{63}$, 209 (1982).

11. D.E. Holmes, R.T. Chen, K.R. Elliot, C.G. Kirkpatrik, and P.W. Yu,
    "Compensation Mechanism in Liquid Encapsulated Czochralski GaAs:
    Importance of Melt Stoichiometry," IEEE MTT-$\underline{30}$, 949 (1982).

12. P.W. Yu, "Studies on the 0.58-eV Photoluminescence Emissions in Heat-
    treated Semi-insulating GaAs," (Shiva, Nantwich, U.K., 1982) p. 305.

13. D.C. Reynolds, C.W. Litton, E.B. Smith, P.W. Yu, and K.K. Bajaj,
    "Photoluminescence Studies of the Amphoteric Behavior of Carbon and
    Germanium in GaAs," Solid State Commun. $\underline{42}$, 827 (1982).

14. P.W. Yu, "Deep-center Photoluminescence in Undoped Semi-insulating
    GaAs: 0.68-eV Band due to the Main Deep Donor," Solid State Commun.
    $\underline{43}$, 953 (1982).

15. P.W. Yu and D.C. Walters, "Deep Photoluminescence Band Related to Oxygen in GaAs," Appl. Phys. Lett. 41, 863 (1982).

16. P.W. Yu, W.C. Mitchel, M.G. Mier, S.S. Li, and W.L. Wang, "Evidence of Intrinsic Double Acceptor in GaAs," Appl. Phys. Lett. 41, 532 (1982).

17. S. Chaudhuri, "Optical-Transition Cross Sections Involving Impurities in Semiconductors," Phys. Rev. B26, 6593 (1982).

18. W.M. Theis, K.K. Bajaj, C.W. Litton, W.G. Spitzer, "Direct Evidence for the Site of Substitutional Carbon Impurity in GaAs," Appl. Phys. Lett. 41, 70 (1982).

19. D.C. Look, "The Electrical and Photoelectronic Properties of Semi-Insulating GaAs," Semiconductors and Semimetals, Vol. 19 (ed. by R.K. Willardson and A.C. Beer) pp. 75-170 (1983).

20. D.C. Look and Gernot S. Pomrenke, "A Study of the 0.1eV Conversion Acceptor in GaAs," J. Appl. Phys. 54, 3249 (1983).

21. D.C. Look, L. Chaudhuri, and J.R. Sizelove, "Defect Nature of the 0.4eV Center in O-doped GaAs," Appl. Phys. Lett. 42, 829 (1983).

22. H.J. Lee and D.C. Look, "Hole Transport in Pure and Doped GaAs," J. Appl. Phys. 54, 4446 (1983).

23. S. Chaudhuri and D.C. Look, "Effect of the Velocity-Field Peak on I-V Characteristics of GaAs FET's," Solid State Electronics 26, 811 (1983).

24. D.C. Look and P.C. Colter, "Electrical Properties of Low-Compensation GaAs," Phys. Rev. B28, 1151 (1983).

25. P.C. Colter, D.C. Look, and D.C. Reynolds, "Low-Compensation Vapor-Phase Epitaxial GaAs," Appl. Phys. Lett. 43, 282 (1983).

26. D.C. Walters, D.C. Look, and T.O. Tiernan, "Spark-Source Mass Spectrographic Analysis of GaAs for Trace O and C using Liquid-Helium Cryopumping," Analytical Letters 16, A17 (1983).

27. P.W. Yu, "Photoluminescence Excitation of the 1.44-eV Cation Antisite Emission in p-type GaAs," Phys. Rev. B27, 7779 (1983).

28. S. Chaudhuri, D.D. Coon, and G.E. Derkits, "Solid Solutions of Fractional Z Elements in Tetrahedrally Bonded Crystals," Physica Scripta. 27, 23 (1983).

29. S. Chaudhuri, D.D. Coon, and R.P.G. Karunasiri, "Impurity-to-Band Tunneling in Semiconductors," J. Appl. Phys. 54, 5476 (1983).

30. S. Chaudhuri, "Hydrogenic-Impurity Ground State in GaAs-Ga$_{1-x}$Al$_x$As Multiple-Quantum-Well Structures," Phys. Rev. B28, 4480 (1983).

31. S. Chaudhuri and F. Keffer, "Classical and Quantum Theory of Radiation Linewidth in Ferromagnetic and Antiferromagnetic resonance," J. Phys. Chem. Solids, in press (1983).

32. W.M. Theis, K.K. Bajaj, C.W. Litton, W.G. Spitzer, "Direct Evidence for the Site of Substitutional Carbon in GaAs using Localized Vibrational Mode Spectroscopy," Physica $117B$, 116 (1983).

33. P.W. Yu and E. Kuphal, "Photoluminescence of Mn- and Un-doped $Ga_{0.47}-In_{0.53}As$ on InP," Solid State Commun., 1984.

34. P.W. Yu, "Persistent Photoluminescence Quenching of 0.68-eV Emission in Undoped Semiinsulating GaAs," Appl. Phys. Lett., 1984.

35. P.W. Yu, "Photoluminescence Excitation of the 0.77-eV Emission in Undoped Semiinsulating GaAs," Phys. Rev. $\underline{B}$, 1984.

36. S. Chaudhuri and K.K. Bajaj, "Effect on Non-parabolicity on the Energy Levels of Hydrogenic Impurity States in GaAs $Ga_{1-x}Al_xAs$ Quantum-Well Structures," Phys. Rev. $\underline{B}$, 1984.

37. J. Singh, K.K. Bajaj, and S. Chaudhuri, "Theory of Photoluminescence Lineshape Due to Interfacial Quality in Quantum Well Structures," Appl. Phys. Lett., 1984.

38. D.E. Phelps and K.K. Bajaj, "Screening Effects on the D^- System in Semiconductors." Phys. Rev. $\underline{B26}$, 912 (1982).

39. G.B. Norris and K.K. Bajaj, "Exciton-Plasma Transition in Si." Phys. Rev. $\underline{B26}$, 6706 (1982).

40. D.E. Phelps and K.K. Bajaj, "Effect of Free Carrier Screening on the Binding Energy of D^- centers in Polar Semiconductors." Solid State Commun. $\underline{45}$, 121 (1983).

41. Ronald L. Greene and K.K. Bajaj, "Energy Levels of Hydrogenic Impurity States in GaAs-GaAℓAs Quantum Well Structures." Solid State Commun. $\underline{45}$, 825 (1983).

42. Ronald L. Greene and K.K. Bajaj, "Binding Energies of Wannier Excitons in GaAs-GaAℓAs Quantum Well Structures." Solid State Commun. $\underline{45}$, 831 (1983).

43. D.E. Phelps and K.K. Bajaj, "Effect of Screening Due to Free Mobile Charges on the Binding Energy of an H^- Ion." Astrophysical Journal, 268, 447 (1983).

FILMED